NASA/TM—2019-220147

Microgravity Liquid-Gas Two-Phase Flow: Review of Pressure Drop and Heat Transfer Correlations and Guidelines for Equipment Operability

R. Balasubramaniam
Case Western Reserve University, Cleveland, Ohio

Enrique Ramé
Universities Space Research Association, Cleveland, Ohio

Brian J. Motil
Glenn Research Center, Cleveland, Ohio

March 2019

NASA STI Program . . . in Profile

Since its founding, NASA has been dedicated to the advancement of aeronautics and space science. The NASA Scientific and Technical Information (STI) Program plays a key part in helping NASA maintain this important role.

The NASA STI Program operates under the auspices of the Agency Chief Information Officer. It collects, organizes, provides for archiving, and disseminates NASA's STI. The NASA STI Program provides access to the NASA Technical Report Server—Registered (NTRS Reg) and NASA Technical Report Server—Public (NTRS) thus providing one of the largest collections of aeronautical and space science STI in the world. Results are published in both non-NASA channels and by NASA in the NASA STI Report Series, which includes the following report types:

- TECHNICAL PUBLICATION. Reports of completed research or a major significant phase of research that present the results of NASA programs and include extensive data or theoretical analysis. Includes compilations of significant scientific and technical data and information deemed to be of continuing reference value. NASA counter-part of peer-reviewed formal professional papers, but has less stringent limitations on manuscript length and extent of graphic presentations.

- TECHNICAL MEMORANDUM. Scientific and technical findings that are preliminary or of specialized interest, e.g., "quick-release" reports, working papers, and bibliographies that contain minimal annotation. Does not contain extensive analysis.

- CONTRACTOR REPORT. Scientific and technical findings by NASA-sponsored contractors and grantees.

- CONFERENCE PUBLICATION. Collected papers from scientific and technical conferences, symposia, seminars, or other meetings sponsored or co-sponsored by NASA.

- SPECIAL PUBLICATION. Scientific, technical, or historical information from NASA programs, projects, and missions, often concerned with subjects having substantial public interest.

- TECHNICAL TRANSLATION. English-language translations of foreign scientific and technical material pertinent to NASA's mission.

For more information about the NASA STI program, see the following:

- Access the NASA STI program home page at http://www.sti.nasa.gov

- E-mail your question to help@sti.nasa.gov

- Fax your question to the NASA STI Information Desk at 757-864-6500

- Telephone the NASA STI Information Desk at 757-864-9658

- Write to:
  NASA STI Program
  Mail Stop 148
  NASA Langley Research Center
  Hampton, VA 23681-2199

NASA/TM—2019-220147

Microgravity Liquid-Gas Two-Phase Flow: Review of Pressure Drop and Heat Transfer Correlations and Guidelines for Equipment Operability

R. Balasubramaniam
Case Western Reserve University, Cleveland, Ohio

Enrique Ramé
Universities Space Research Association, Cleveland, Ohio

Brian J. Motil
Glenn Research Center, Cleveland, Ohio

National Aeronautics and
Space Administration

Glenn Research Center
Cleveland, Ohio 44135

March 2019

Acknowledgments

The authors thank John B. McQuillen, Low-Gravity Exploration Technology Branch (LTX), NASA Glenn Research Center, for his technical assistance and critical review comments.

Level of Review: This material has been technically reviewed by technical management.

Available from

NASA STI Program
Mail Stop 148
NASA Langley Research Center
Hampton, VA 23681-2199

National Technical Information Service
5285 Port Royal Road
Springfield, VA 22161
703-605-6000

This report is available in electronic form at http://www.sti.nasa.gov/ and http://ntrs.nasa.gov/

Microgravity Liquid-Gas Two-Phase Flow: Review of Pressure Drop and Heat Transfer Correlations and Guidelines for Equipment Operability

R. Balasubramaniam
Case Western Reserve University
Cleveland, Ohio 44106

Enrique Ramé
Universities Space Research Association
Glenn Research Center
Cleveland, Ohio 44135

Brian J. Motil
National Aeronautics and Space Administration
Glenn Research Center
Cleveland, Ohio 44135

Abstract

In this report we have catalogued the flow regimes observed in microgravity, summarized correlations for the pressure drop and rate of heat transfer that are commonly used, and discuss the validation of a few correlations from available experimental results. Two-phase flow through some specific components such as bends, tees, filters and pumps are discussed from a physical perspective to guide the designer on how reduced gravity might affect their performance. Phase separation in zero gravity is addressed through the behavior and basic design concepts for devices based on passive centrifugal action, capillary forces, gas extraction through a membrane installed in a channel wall and the use of a syringe with a perforated piston to remove bubbles from small liquid volumes. We address the common instabilities that develop in flow loops owing exclusively to the two-phase nature of the flow, e.g., Ledinegg instability and concentration waves. Finally we briefly review flow metering and gauging; two-phase flow through porous media, where pressure drop and flow regime map correlations in zero-g are a current research topic; and basic operation principles of heat pipes and capillary pumped loops.

Table of Contents

Table of Contents **2**

1 Introduction to two phase flow **4**
1.1 Background . . . 4
1.2 Description of two phase flow . . . 5
1.3 Microgravity two phase flow features . . . 6
1.4 Typical two phase flow system . . . 6

2 Dimensionless parameters **6**
2.1 Buckingham Pi theorem . . . 6
2.2 Scaling analysis of governing equations . . . 7
2.3 Parameter ranges for typical applications . . . 9
2.4 Conditions for g-independent operation and ground testability . . . 9

3 Reduced gravity flow regimes **10**
3.1 Description of regimes . . . 10
3.2 Regime transition criteria . . . 10
3.2.1 Bubble-slug transition . . . 10
3.2.2 Slug-annular transition . . . 12
3.3 Other flow regime transition criteria . . . 12
3.3.1 Gas void fraction criterion . . . 12
3.3.2 Weber number criterion . . . 13
3.4 Transition mechanisms . . . 13
3.4.1 Mechanisms for bubble-slug and slug-annular transition . . . 13
3.5 Merits and demerits of each regime for components/system . . . 14

4 Pressure Drop Predictions **15**
4.1 Homogeneous fluid model . . . 15
4.1.1 Pressure drop due to flow acceleration . . . 15
4.1.2 Pressure drop due to wall friction . . . 15
4.2 Regime specific models . . . 16
4.2.1 Separated flow model . . . 16
4.2.2 Pressure drop in bubbly flow . . . 18
4.2.3 Pressure drop in slug flow . . . 18
4.2.4 Comparison of microgravity pressure drop with Lockhart-Martinelli and Friedel predictions . . . 19
4.3 Pressure drop for fully developed, laminar, annular flow . . . 19
4.3.1 Pressure drop due to wall friction in zero gravity . . . 20
4.3.2 Pressure drop due to flow acceleration . . . 20

5 Heat transfer in reduced gravity two phase flows **21**
5.1 Single phase flow . . . 21
5.2 Two phase flow without phase change . . . 23
5.2.1 Homogeneous flow . . . 23
5.2.2 Annular flow . . . 23
5.3 Flow with phase change . . . 24
5.3.1 Chen correlation . . . 25

5.3.2 Kim and Mudawar correlation . . . 26
5.3.3 Heat transfer correlation for condensation in tubes . . . 26
5.3.4 Validity of flow boiling heat transfer correlations in low gravity . . . 26

6 Two phase flow through specific components 27
6.1 Bends, tees, expansion and contraction . . . 27
6.1.1 Bends . . . 27
6.1.2 Expansions . . . 27
6.1.3 Contractions . . . 27
6.1.4 Tees . . . 28
6.2 Separator . . . 28
6.2.1 Centrifugal cyclonic separator . . . 28
6.2.2 Capillary flow separation . . . 29
6.2.3 Membrane separation . . . 29
6.2.4 Removal of bubbles from a small liquid volume . . . 31
6.2.5 Moving unwanted bubbles in systems . . . 33
6.3 Filter . . . 33
6.4 Pumps . . . 34

7 Startup, transients and system instabilities 34
7.1 Ledinegg instability . . . 35
7.1.1 Basic principles and simple model . . . 35
7.1.2 Model results . . . 37
7.2 Concentration waves . . . 37
7.3 Dynamic instabilities: cavitation . . . 39

8 Other topics 39
8.1 Flow metering and mass gauging . . . 39
8.2 Flow through porous media . . . 41
8.2.1 Friction factors and pressure drop . . . 41
8.2.2 Flow regime maps . . . 42
8.2.3 Open aspects in zero-G . . . 43
8.3 Heat pipes and capillary pumped loops . . . 44

1 Introduction to two phase flow

Two-phase flow commonly refers to the simultaneous flow of gas and liquid in flow systems. They occur in many space systems, such as those used for regenerative life support, power generation, thermal control, and storage and transfer of cryogens. Two-phase flows are critical to regenerative life support technologies, specifically to reclaim and process water, generate oxygen, and revitalize cabin atmosphere. The production of food from plants on extended space voyages has its challenges on water, air and nutrient feed systems for plant growth.

Two-phase flow, and multiphase flow of gas, liquid and solid, have been identified and given high priority in the final report of a workshop on critical issues in microgravity fluids, transport and reaction processes [1]. Many review panels have advocated that NASA must develop physically based predictive tools for low gravity multiphase systems and associated transport processes (see, for example [2, 3]).

In this report we have catalogued the flow regimes observed in reduced gravity, and summarized available correlations for the pressure drop and rate of heat transfer. Two-phase flow in some common subsystems are addressed from a physical perspective to guide a designer. To write this report we have have used information from published knowledge, analysis of basic equations that describe flow and information gathered from technical reports by ETH (the Swiss Federal Institute of Technology) [4], Lahey [5], Crowley and Izenson [6], and Mudawar [7]. We have used material liberally from our previous work on two-phase flows [8].

1.1 Background

Multiphase technology is likely to become necessary in regenerative life support systems in extended missions to destinations outside low earth orbit because it will not be possible to carry all the resources needed for the trip. Two-phase technologies are not routinely implemented by system designers in low gravity because of a lack of technology demonstration and therefore lack of confidence in predictive models. For example, the ISS uses a single phase external ammonia loop for thermal control, as well as single phase water loops for internal heat acquisition. However, several two-phase solutions for the ammonia loop were initially proposed [9].

Lahey and Dhir [3] mention that future NASA missions will require significantly higher power levels than in the past. They advocate the use of a nuclear reactor power plant using the Rankine cycle as the power source. A single phase, flowing liquid metal loop is employed as the primary coolant. It exchanges energy with a secondary two-phase loop of an appropriate working fluid to drive a turbine to generate power. The two-phase loop is required so that heat rejection via radiators is at near constant temperature, and enables higher radiator temperatures, lower system volume and mass, lower reactor operating temperatures, and relatively higher energy conversion efficiency.

The two-phase flow technologies, however, are not without their issues. A number of reports, [2, 3], describe significant design challenges in low gravity two-phase systems because of unique liquid-vapor shapes and how the phases are distributed. The lack of gravity profoundly influences the shape of interfaces and bubbles and their interaction among each other and with the flowing liquid. This implies that new models of two phase flow behavior must be built and validated, and design principles established based on the know-how to ensure system operation, prevent unwanted behavior, and improve efficiencies. We are all familiar with the spacesuit helmet leak that nearly drowned an ISS astronaut in 2013 [10]. Another water leak happened on January 15, 2016 [11].

Two phase flow in space systems can occur over vastly different length scales. The EVA suit example given above, the on-orbit mixing and generation of fluids for intravenous use in astronauts, and obtaining water samples for water quality testing are examples of small scale systems. We mention these examples because unwanted gas bubbles and liquid drops have been frequently observed in such applications. Systems used for life support and environmental control are medium sized systems. The typical water needs of an astronaut are in the tens of kilograms per day, including water for metabolic needs, personal hygiene, and washing clothes and dishes [12]. Water recovery systems that reclaim and process wastewater from urine, cabin humidity condensate, oxygen generation systems that electrolyze water, and air revitalization systems for humidity control, carbon dioxide reduction etc, all must use multiphase flow technologies.

The largest systems are expected to be those used for power generation in future spacecraft. For reference, the External Active Thermal Control System on the ISS that uses liquid ammonia as the working fluid has two loops each capable of collecting, transporting and rejecting 35 KW of heat, and contains 640 pounds of ammonia. The Internal Active Thermal Control System uses a Low Temperature Loop that contains 63 liters of water, and a Moderate Temperature Loop that contains 200 liters of water. Both the internal and external loops are quite massive, use single-phase liquid and contain many subsystems.

1.2 Description of two phase flow

In two phase flow, two phases, typically gas and liquid flow through a system, such as a pipe, simultaneously. Because the liquid/gas interface can deform, the location of the regions occupied by gas and liquid in the pipe is unknown to begin with and is of great interest in designing the two phase flow system. Some of the common states of the two phases are: (i) *bubbly flow*, in which the gas is present within the liquid in the form of innumerable bubbles of small size (ii) *slug flow* where individual gas bubbles merge to form a large gas mass or slug that is often cylindrical in shape. Sometimes the cylindrical gas bubbles are called Taylor bubbles, and the liquid separating two such bubbles liquids slugs or simply slugs. (iii) *separated or stratified flow* where the gas and liquid regions are separated, with the gas that is lighter flowing on top of the heavier liquid in normal gravity (iv) *annular flow* where one fluid (typically the liquid) occupies the space adjacent to the tube wall and surrounds the other fluid (gas) that flows in the center of the tube. Where the liquid is, where the gas is, and in what form, is determined from a flow regime map. Such a map attempts to connect the observations made of the state of the two phase flow to the tube size, physical properties of the liquids, and the rates at which the liquid and gas flow. The liquid and gas flow rates are often specified in terms of superficial velocities, which is the velocity of the liquid or gas if it alone flows through the pipe. The void fraction refers to the fraction of the space occupied by the gas in a region within the pipe. Especially of interest to the designer is the pressure drop as the two phases flow through the pipe, and in the case of non-isothermal systems, the rate at which heat can be transported in the pipe by the two phase flow.

1.3 Microgravity two phase flow features

From reduced gravity experiments that have been conducted, typically aboard aircraft, the following general features of two-phase flow have been observed.

- Two phase flow in pipes exhibit the axisymmetric flow regimes of bubble, slug and annular flow. Separated flow, which is commonly observed in horizontal flows in normal gravity, have not been detected in low gravity.
- Bubbles are held in place relative to each other longer in low gravity and are thus prone to more coalescence, especially for slow flows.
- The lower inertia of the gas phase enables it to change direction much more readily than the liquid, as well as render the gas to be sheared or pushed off from solid surfaces by the inertia of the flowing liquid.
- Gas bubbles can get trapped in zones of small size where the flow recirculates.

1.4 Typical two phase flow system

Two phase flows usually require a pressure differential or thermal gradient to move the flow through the system. While a two-phase pump can be used, it seldom is, and a single phase pump to move the liquid is most common. There is also a source of gas, produced for example by some chemical process, or by phase change due to the addition of heat. Scientific studies performed to observe flow behavior typically use a gas bottle as the external gas source. The transport of the flow usually occurs in pipes. There are valves to control flow rates, and filters to remove particulate matter from the liquid. System pressure is usually maintained by an accumulator or liquid reservoir whose pressure is controlled. Heaters or heat exchangers may be present to control temperatures. A liquid/gas separator is used to separate the phases, which are recycled through the system, or vented to the outside. Temperature and pressure sensors, and meters to detect flow rates are used to sense the state of the system. Two phase flow in some specific components in the system that are affected by the gravitational level are described in Section 6.

2 Dimensionless parameters

We will consider two-phase flow phenomena when the two phases are being transported via a pipe or a channel from one reservoir to another. In what follows we only deal with isothermal flow of gas and liquid. A knowledge of the dimensionless parameters in two phase flow is useful because, as in single phase flow, it can enable theoretical and experimental results for a particular flow situation (fluids, tube size, velocities, gravity level etc.) to be scaled and extrapolated to a different flow situation. Quite often, casting results in terms of dimensionless parameters can also provide a clue to the underlying physical mechanisms.

2.1 Buckingham Pi theorem

In the absence of phase change, the independent variables are:

$$U_{LS},\ U_{GS},\ \mu_L,\ \mu_G,\ \rho_L,\ \rho_G,\ D, \text{ and } \sigma. \tag{1}$$

These symbols denote the superficial liquid velocity, superficial gas velocity, liquid viscosity, gas viscosity, liquid density, gas density, pipe diameter, surface tension. The superficial velocity is the

average velocity each phase would have if it alone flows in the pipe. There are eight variables and three fundamental units (mass, length and time). Using the Buckingham Pi theorem, this yields five independent dimensionless parameters. One set of dimensionless parameters is:

$$Re_L = \frac{\rho_L U_{LS} D}{\mu_L},\ Re_G = \frac{\rho_G U_{GS} D}{\mu_G},$$
$$We_L = \frac{\rho_L U_{LS}^2 D}{\sigma},\ \frac{\mu_G}{\mu_L},\ \frac{\rho_G}{\rho_L} \tag{2}$$

where Re_L is the liquid Reynolds number, Re_G is the gas Reynolds number, We_L is the Weber number in the liquid. A commonly used parameter is the slip ratio defined as:

$$S = \frac{U_{GS}}{U_{LS}}. \tag{3}$$

S may be derived from the liquid and gas Reynolds numbers, and the density and viscosity ratios. One other dimensionless parameter derivable from the above set is the Suratman number:

$$Su = \frac{Re_L^2}{We_L} = \frac{\rho_L D \sigma}{\mu_L^2} \tag{4}$$

that has been used in the literature and is important in demarcation of flow regime transition boundaries in low gravity. A question arises as to what the natural set of five dimensionless parameters is. To determine these, we perform a scaling analysis of the governing equations for two phase flow in the absence of heat transfer.

2.2 Scaling analysis of governing equations

The governing equations for two phase flow that we consider are the incompressible Navier-Stokes equations. They are written separately for the liquid and gas phase below.

$$\rho_L \left(\frac{\partial \mathbf{U}_L}{\partial t} + \mathbf{U}_L \cdot \nabla \mathbf{U}_L \right) = -\nabla p_L + \mu_L \nabla^2 \mathbf{U}_L \tag{5}$$

$$\rho_G \left(\frac{\partial \mathbf{U}_G}{\partial t} + \mathbf{U}_G \cdot \nabla \mathbf{U}_G \right) = -\nabla p_G + \mu_G \nabla^2 \mathbf{U}_G \tag{6}$$

where $\mathbf{U}$ is velocity, p is pressure and the subscripts L, G refer to the liquid and the gas, respectively.

We choose the following reference quantities to normalize the variables.

- Gas velocity: U_{GS} = Superficial gas velocity
- Liquid velocity: U_{LS} = Superficial liquid velocity
- Time: $\frac{D}{U_L}$

- Length: D = pipe diameter
- Gas pressure: $\rho_L U_{LS}^2$
- Liquid pressure: $\rho_L U_{LS}^2$

Before we proceed we discuss the choice for the pressure normalization given above. Both the liquid and gas pressures are referred to the same datum (the pressure in the liquid at any cross-sectional plane) and is scaled by $\rho_L U_{LS}^2$. Consider a two phase flow in which the liquid forms the continuous phase, and contains many gas bubbles as the dispersed phase. We expect the pressure within a gas bubble to be equal to the pressure in the liquid surrounding it, except for a contribution arising from surface tension. Thus the gas and liquid pressures adjacent to the liquid/gas interface are approximately the same. The normalization scheme we have chosen for the pressures reflects this idea. If drops of liquid are present in a gas as the continuous phase, the density of the gas ρ_G and its superficial velocity U_{GS} must be used in normalizing the pressure in the liquid and gas. The pressure normalization factors in the liquid and gas can be different for stratified flow and developing or entrance flows. The scaling analysis performed here is not valid for such situations and must be suitably modified.

With these choices the governing equations can be written in the following dimensionless form.

$$\frac{\partial \mathbf{u}_L}{\partial t} + \mathbf{u}_L \cdot \nabla \mathbf{u}_L = -\nabla p_L + \frac{1}{Re_L} \nabla^2 \mathbf{u}_L \tag{7}$$

$$S\frac{\partial \mathbf{u}_G}{\partial t} + \mathbf{u}_G \cdot \nabla \mathbf{u}_G = -\nabla p_G + \frac{1}{Re_G} \nabla^2 \mathbf{u}_G. \tag{8}$$

We next look at the balance of shear and normal stresses at the liquid/gas interface. When the surface tension is uniform (i.e., no Marangoni stress at the interface), the balance of shear stress yields

$$\left(\frac{\mu_L U_{LS}}{\mu_G U_{GS}}\right) \frac{\partial u_L}{\partial s} = \frac{\partial u_G}{\partial s} \tag{9}$$

where s is distance tangential to the interface. The balance of normal stress may be written as

$$We_L \left(p_G - p_L\right) + 2\, Ca \left(\frac{\partial u_{Ln}}{\partial n} - \frac{\mu_G U_{GS}}{\mu_L U_{LS}} \frac{\partial u_{Gn}}{\partial n}\right) = 2H \tag{10}$$

where $Ca = \frac{\mu_L U_{LS}}{\sigma}$ is the Capillary number, H is the mean curvature of the interface and n is distance normal to the interface.

Thus the scaling analysis reveals that the dimensionless parameters in two phase flow are the gas and liquid Reynolds numbers, the slip ratio, the viscosity ratio, and the liquid phase Weber number. The density ratio can be derived from the above dimensionless groups.

When the cross section of the flow duct is not circular, the hydraulic diameter,

$$D_h \equiv \frac{4 \times Flow\ Area}{Flow\ perimeter}$$

should be used instead of D to calculate the Reynolds number. Note that the velocity should be calculated by dividing the volumetric flow rate by the actual area of cross section of the duct, and not by using the hydraulic diameter.[1]

2.3 Parameter ranges for typical applications

Balasubramaniam *et al.* (2006) [8] provide estimates of the Suratman number, and liquid and gas Reynolds numbers for some low gravity technologies for water and air management. The water and air flow rates are approximately in the range 8 to 35 and 0.02 to 3 kg/day, respectively. One system with a very high air flow rate of nearly 12000 kg/day is the condensing heat exchanger used for humidity control. The high value arises from the requirements on the recirculation of the ISS cabin air. Excluding this application, and assuming a nominal pipe diameter of 0.64 cm in which two-phase flow occurs, the estimates for the dimensionless parameters are $Su = 4.5 \times 10^5$, $Re_G < 700$, and $Re_L < 80$ in low gravity water recovery technologies.

2.4 Conditions for g-independent operation and ground testability

Ungar *et al.* 1998 [16] argue based on analysis of dimensionless parameters that it should be possible to simulate microgravity conditions on Earth using systems similitude. It is not clear from this work whether microgravity flow regime maps can be obtained on Earth under wholly similar conditions.

The gravitational acceleration influences the two-phase system via the Froude number and the orientation angle of the pipe relative to the horizontal. We may infer that the effects of g on the system behavior might be negligible when the Froude number is negligibly small. Note that for tests in normal gravity the larger of $Fr_G = (\Delta\rho/\rho_G)(gD/U_{GS}^2)$ and $Fr_L = (\Delta\rho/\rho_L)(gD/U_{LS}^2)$ should be small ($\Delta\rho \equiv \rho_L - \rho_G$). Besides, the system behavior should be tested for all orientations – horizontal flow and vertical upflow and downflow. If the effects of gravity are truly negligible, all these tests should yield the same system behavior. There are some limitations, however, in inferring gravity independent behavior from normal gravity testing. Only gross features of the flow can be obtained – since the gravitational force is a body force, it affects every region of the flow system, including places where the flow velocities are low. In these regions the local Froude number may not be small, and the system behavior in low g and normal g may be different. Also, the testing in normal gravity for some systems may require larger flow velocities than intended for low g operation; not only is the effect of gravity altered when the flow speed is different, but also the balance with other forces such as surface tension. Even if the flow speeds in low g and normal g testing are the same, the system behavior during startup and shutdown might be different as the slow speeds are traversed, where the influence of the gravitational force increases; and this in turn may affect the test state. For these reasons, the normal gravity test results for g independent operation should be interpreted cautiously. There is no substitute for actual reduced gravity testing using the drop tower, low g aircraft, or the ISS.

Zhang, Mudawar and Hasan (2004) [17] have come up with criteria to determine the importance of gravity on the critical heat flux (CHF) in flow boiling. They measured the CHF for channel flow of the fluid FC-72 with orientations of the g vector from 0 to 360 deg in 45 deg increments. The measurements compared favorably with a theoretical model (termed the Interfacial Lift-Off Model).

[1] The hydraulic diameter is used commonly for non-circular duct flows in normal gravity. For reduced gravity flows, Wölk *et al.* (1999) [13] use the hydraulic diameter to classify flow regimes. Also, Fang *et al.* (2012) [14] use the hydraulic diameter in interpretation of the data of Zhao *et al.* (2001) [15] for a square channel.

Based on this comparison, and the fact that the experimental results showed little dependence on the orientation for flow velocity of 1.5 m/s, they determined criteria for negligible influence of gravity both parallel ($\|$) and perpendicular ($\perp$) to the heated wall. The criteria are

$$\frac{(\rho_L - \rho_G)(\rho_L + \rho_G)^2 \sigma g_\perp}{\rho_L^2 \rho_G^2 U^4} \leq 0.09 \tag{11}$$

$$\frac{(\rho_L - \rho_G) g_\| D_h}{\rho_L U^2} \leq 0.13 \tag{12}$$

3 Reduced gravity flow regimes

3.1 Description of regimes

Jayawardena *et al.* [18] say that in the absence of gravity three major flow patterns exist – bubbly flow, slug flow and annular flow, with annular flow being obtained for a wide range of gas and liquid flow rates. For a fixed liquid flow rate, bubbly flow is obtained for low gas flow rates. This regime transitions to slug flow for higher gas flow rates. As the flow rate of the gas increases further, annular flow is obtained. For the operation of two phase flow systems, bubbly and annular flow are preferred. Because slug flow can cause vibrations, it is usually avoided. Typically, the annular flow regime yields maximum volumetric flow rates for a given two-phase system.

In bubbly flow, bubble sizes are relatively uniform, and the bubbles are distributed everywhere in the flow. Slug flow results from the merging and coalescence of individual bubbles, and the bubbles are elongated and more cylindrical in shape (Taylor bubble). The elongated gas bubbles are separated by liquid slugs. Small bubbles are often present in the liquid slugs.

In typical annular flow, the gas occupies the central or core region of the tube, with the liquid remaining in a thin layer adjacent to the tube wall. Waves are present on the liquid/gas interface and the instantaneous shape of the interface fluctuates with time. Also, small liquid drops are typically entrained by the flowing gas. Figure 1 shows pictures of bubbly, slug and annular flow obtained in low gravity.

For gas-liquid flows, the gas/liquid density and viscosity ratios typically have small values. One can therefore surmise that these two property ratios will only have a small influence on the flow. We are thus left with three dimensionless parameters – the gas and liquid Reynolds numbers and the Weber number. This is the starting point of Jayawardena *et al.* [18] in the representation of the flow regime map in terms of dimensionless parameters.

3.2 Regime transition criteria

3.2.1 Bubble-slug transition

Jayawardena *et al.* [18] report that the transition from bubbly flow to slug flow can be written as follows.

$$\left(\frac{Re_G}{Re_L}\right)_{transition} = 464.16\ Su^{-2/3} \tag{13}$$

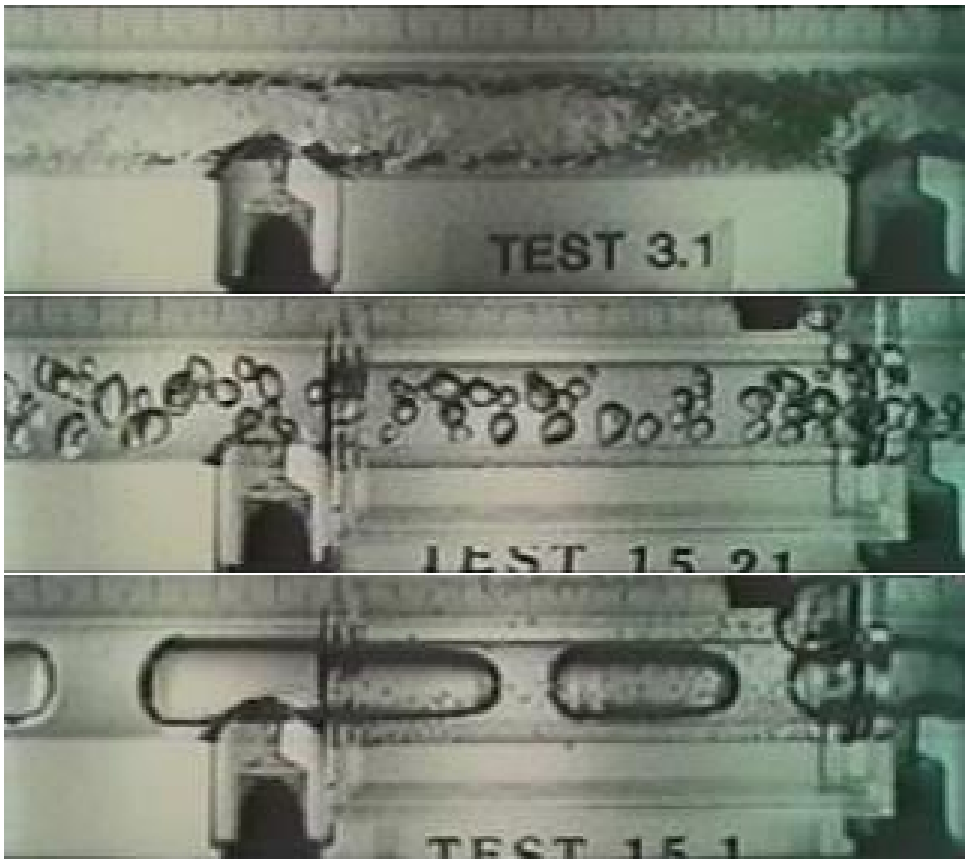

Figure 1: Annular, bubbly and slug flow in reduced gravity (McQuillen *et al.* [19]).

It may also be written alternatively as

$$(Re_G)_{transition} = 464.16\, Ca^{2/3}\, Re_L^{1/3} \tag{14}$$

3.2.2 Slug-annular transition

Jayawardena *et al.* find that the transition from slug flow to annular flow can be written as follows.

$$\left(\frac{Re_G}{Re_L}\right)_{transition} = 4641.6\, Su^{-2/3} \qquad Su < 10^6 \tag{15}$$

$$(Re_G)_{transition} = 2 \times 10^{-9}\, Su^2 \qquad Su > 10^6 \tag{16}$$

Note that for $Su < 10^6$ the slug-annular transition occurs at a Reynolds number ratio that is a factor of 10 greater than the bubble-slug transition Reynolds number ratio. Jayawardena *et al.* [18] show that their map agrees well with nine different experiments in the open literature that used six different fluid pairs (air/water, air/water-glycerin, air/water-zonyl, R11 vapor/liquid, R12 vapor/liquid, R114 vapor/liquid) and ten different tube sizes in the range 4.7 mm to 40 mm. Specifically, the accuracy of bubble-slug transition predictions is 87%, and that for slug-annular transition is 97%.

3.3 Other flow regime transition criteria

Jayawardena *et al.*'s [18] Suratman number based flow regime map is not the only map developed for reduced gravity two-phase flow. In this section we summarize some alternative regime maps.

3.3.1 Gas void fraction criterion

Bousman's thesis [20] details the use of the Drift-flow model to estimate gas void fraction, ϵ_{GA}, knowing the superficial velocities, resulting in a relation $\epsilon_{GA} = F(U_{GS}/U_{LS})$. Since they also measured the void fraction at various flow regimes transitions, $\epsilon_{GA_{Tr}}$, they can plot the regime transition predicted from the Drift-flow model, $U_{GS} = U_{LS}\, F^{-1}(\epsilon_{GA_{Tr}})$ over the measured data. Note that the model only allows a straight line to be the flow regime boundary. The drift-flow model is adequate for predicting bubbly-to-slug transition.

Bousman also uses the drift-flow model coupled with a force balance in the annular flow to describe the slug-to-annular boundary. In this approach, expressions for the void fractions in the slug and in the annular regimes are equated. This yields a relation for the transition superficial velocities. The evaluation of the annular flow void fraction requires the calculation of the interfacial shear at the liquid-gas interface of the annular flow. This is done using a Blasius type friction factor correlation. The Blasius correlation assumes no-slip of the relevant flow phase; whereas the gas does slip on the liquid. However, because typically $U_{GS} \gg U_{LS}$ in annular flow, the error from assuming that the gas does not slip may be small.

The arguments used to derive these boundaries hinge on a parameter C_o that appears in the drift-flow model. This parameter depends on whether the flow in the liquid is laminar or turbulent. The fact that the values of C_o chosen to adjust the data are not always consistent with the values prescribed based on the turbulence level of the liquid, weakens the power of this technique.

3.3.2 Weber number criterion

The Weber number criterion postulates that at the slug-to-annular transition inertial and surface tension forces should both be important. This criterion uses the gas superficial Weber number. It postulates that at transition $We_G = U_{GS}^2 \rho_G D/\sigma \approx 1$. Bousman has tested this criterion with three different fluid systems and two pipe diameters. The changes in fluid systems test the effects of viscosity and surface tension. Changes in pipe diameter test, obviously, the dependence on D. A change in viscosity does not change We_G. If there were a dependency of the transition threshold on μ, it should appear as a shift in We_G between the two systems with different viscosities. The data hint at some viscosity dependence of the transition We_G, although it is difficult to be definite when the scatter is as large as in these data and no error bars are quoted. When the viscosity is constant and D and σ change, the transition We_G seems to hold more or less constant. This supports the Weber-number transition criterion. Comparing the Weber number criterion to the Suratman number criterion of Jaywardena *et al.* [18], the latter has a much sharper demarcation of the flow domains.

3.4 Transition mechanisms

Mechanistic explanations for regime transitions have been attempted for many years. Here we summarize the more relevant ones.

3.4.1 Mechanisms for bubble-slug and slug-annular transition

Two interrelated mechanisms that have been proposed [4] are: (i) coalescence of individual bubbles leading to spherical cap and Taylor bubbles. It is believed that the frequency of bubble collisions, necessary for their eventual coalescence, increases rapidly when the void fraction is larger than 0.2. This led to the belief that bubble-slug transitions occur at void fractions around 0.25. (ii) Since bubble coalescence is a slow process that must be preceded by drainage of the intervening liquid film, it is not very clear that void fraction is the only factor – the coalescing bubbles must be held in place for a sufficiently long time without relative motion. Therefore it has been suggested that the existence of "void waves" which creates regions of large bubble concentration where bubble separation is inhibited is an essential step. Colin *et al.* [21] suggest that coalescence happens more readily in reduced gravity because of lack of relative motion between the gas and the liquid. Thus coalescing bubbles could be held in place longer in reduced gravity.

Jayawardena *et al.* [18] do not discuss any mechanisms for the transition of bubbly to slug flow or from slug to annular flow. It is significant that the data is correlated by the Suratman number, $Su = \frac{\rho_L D\sigma}{\mu_L^2}$. Su only depends on the properties of the liquid and the pipe diameter, and does not depend on the flow rates of the liquid or gas. Briefly, Su is a modified Reynolds number where the characteristic velocity is the "capillary" velocity σ/μ. Thus, increasing surface tension should be thought of as increasing inertia of the capillary-driven flow. There is a likely analogy with breakup of a liquid filament, where the stability limit is controlled by Su. This should be so because it is commonly believed that bubbly-slug and slug-annular transitions are governed by merging and coalescence of bubbles, which are surely influenced by surface tension (and perhaps viscosity).

Another issue concerning transition boundaries is the question of reversibility. Is the transition boundary from regime 1 to regime 2 the same as from regime 2 to regime 1? The experiments we have found do not address this question. Rather, the gas and liquid flow rates are dialed and the ensuing flow regime is interrogated by the diagnostic method of choice. It is therefore of interest to determine whether the regime boundaries are hysteretic or not.

A qualitative or semi-quantitative understanding of the reason why the flow regime map advocated by Jayawardena *et al.* [18] is so successful needs to be determined. One important reason is that, once the mechanism is understood, extensions for non-negligible values of the Froude number can be contemplated, which will be very useful for predicting flow regime maps in partial gravity.

The effect of gravity on axial development of bubbly flows for low liquid Reynolds numbers in small diameter pipes was studied by Takamasa *et al.* [22, 23] by monitoring key flow parameters such as void fraction, interfacial area concentration, bubble Sauter mean diameter and bubble number density. The flow measurements were performed in an air-water system using a non-intrusive image processing method with three digital cameras placed at 5, 20 and 40 diameters along the pipe section. The microgravity tests were performed in the underground drop shaft facility at the Japanese Microgravity Center (JAMIC) providing 10 s of reduced gravity environment with nearly negligible residuals between 10^{-4} and 10^{-5} g. The main mechanisms for transition from bubbly to slug flow were studied by examining bubble coalescence and breakup. Since for the relatively low Reynolds numbers that prevailed in these studies, bubble breakup was minimal, the main driving force for flow transition was due to bubble coalescence. Considerable bubble coalescence was observed in both the 1g and reduced gravity experiments. Visual records indicate that in 1g the main mechanism for bubble coalescence is wake entrainment. Wake entrainment refers to the entrainment of a trailing bubble by the motion of a leading bubble in the liquid – the motion of the leading bubble sets up a flow in the liquid that tends to entrain other bubbles. In microgravity, however, there is no mechanism for relative motion of the liquid and gas; thus wake entrainment is absent. At low liquid Reynolds numbers, where the flow is basically laminar and the velocity profile is parabolic, Takamasa *et al.* report that velocity profile entrainment is the main mechanism for bubble coalescence. In normal as well as microgravity, due to the relatively low Reynolds numbers encountered, coalescence due to random collisions is minimal. Curiously, it seems that the relative contributions of velocity profile entrainment, in microgravity, and wake entrainment, in 1g, to bubble coalescence is the same. This results in nearly similar flow structure developments for the two environments leading to a decrease in the interfacial area concentration and an increase in the Sauter mean diameter along the pipe.

3.5 Merits and demerits of each regime for components/system

Bubbly flow regime supports only small gas flow rates. The area to volume ratio of the gas, however, is high that enables efficient mass or energy transfer across the liquid-gas interface.

The annular flow regime supports large gas flow rates relative to the liquid. Reasonably steady flow is achieved in this regime. The large gas velocities can lead to wavy interfaces, and strip and entrain liquid drops in the gas core.

The slug flow regime is problematic and inevitably leads to fluctuations in pressure drop, wall shear stress and mass flow as the phase that crosses a reference location in the system alternates between liquid and gas. In terrestrial oil production, slug flow can cause undesirable consequences such as low and high liquid level in liquid/gas separators, flooding, corrosion, varying structural loading and equipment damages (Sausen *et al.*, [24]). Slug flow can also cause erosion in protective coatings on the tube wall in hydrocarbon production lines (Kvernvold *et al.* [25]).

4 Pressure Drop Predictions

The knowledge of pressure drop in a two-phase flow system is important for its design. It enables the designer to size the pump required for the operation of the flow system. We present below the most common approaches in prediction of the pressure drop in two-phase flows.

4.1 Homogeneous fluid model

The pressure gradient in a two-phase flow can be thought of as arising from three additive contributions: (i) frictional (ii) flow acceleration and (iii) hydrostatic head. Thus,

$$\frac{dp^*}{dz^*} = \left(\frac{dp^*}{dz^*}\right)_{fr} + \left(\frac{dp^*}{dz^*}\right)_{ac} + \left(\frac{dp^*}{dz^*}\right)_{gr} \tag{17}$$

In the homogeneous fluid model, the fluid is characterized by an effective fluid that has suitably averaged properties of the liquid and gas phases. In reduced gravity, the hydrostatic head is unimportant and is not considered.

4.1.1 Pressure drop due to flow acceleration

The pressure gradient due to flow acceleration can be written as

$$\left(\frac{dp^*}{dz^*}\right)_{ac} = \frac{d}{dz^*}\left(\frac{1}{A}\int_A \rho u^2 dA\right) = \dot{m}^2 \frac{d}{dz^*}\left(\frac{1}{\rho_H}\right) \tag{18}$$

where $\dot{m}$ is the total rate of mass flow per unit area in the pipe, and the effective density ρ_H is defined by:

$$\rho_H = \epsilon_{GA}\rho_G + (1 - \epsilon_{GA})\rho_L \tag{19}$$

where ϵ_{GA} is the area averaged local void fraction of the gas, ρ_G and ρ_L are the densities of the gas and the liquid.

4.1.2 Pressure drop due to wall friction

The frictional pressure drop due to the shear stress exerted by the tube wall is considered the most problematic term in two-phase pressure drop. The frictional pressure drop may be related to the wall shear stress τ_W by a force balance:

$$\left(\frac{dp^*}{dz^*}\right)_{fr} = \frac{2\tau_W^*}{R} \tag{20}$$

We present various approaches used in the literature to determine the frictional pressure drop.

Friction factor

Analogous to single phase flow, the use of friction factors in determining the two-phase frictional pressure drop is common. A typical expression for the friction factor f is given below.

$$\left(\frac{dp^*}{dz^*}\right)_{fr} = \frac{f\dot{m}^2}{\rho_H R}$$

$$f = 0.079 Re^{-0.25} \tag{21}$$

where the Reynolds number is $Re = \frac{2\dot{m}R}{\mu_H}$ with the effective viscosity approximated as [26]:

$$\mu_H = \mu_L \quad \text{or} \tag{22}$$

$$\mu_H = x\mu_G + (1-x)\mu_L \quad \text{or} \tag{23}$$

$$\frac{1}{\mu_H} = \frac{x}{\mu_G} + \frac{(1-x)}{\mu_L}, \quad \text{or} \tag{24}$$

$$\mu_H = x\left(\frac{\rho_H}{\rho_G}\right)\mu_G + (1-x)\left(\frac{\rho_H}{\rho_L}\right)\mu_L \tag{25}$$

where x is the quality (the gas mass flow fraction) and ρ_H is defined in Eq. 37.

Two-phase friction factor multiplier

Here the frictional pressure gradient for two-phase flow is determined by multiplying the frictional pressure gradient for flow of the liquid alone by a two-phase multiplication factor. The mass flow rate of the single phase liquid flow is the same as that of the liquid in the two-phase flow.

$$\left(\frac{dp^*}{dz^*}\right)_{fr,TP} = \phi_{LO}^2 \left(\frac{dp^*}{dz^*}\right)_{fr,LO} \tag{26}$$

where subscript TP denotes two-phase and LO liquid only. A typical correlation for the two-phase multiplier is [4]

$$\phi_{LO}^2 = \frac{\rho_L}{\rho_H}\left[1 + x\frac{(\rho_L - \rho_G)}{\rho_G}\right]\left[1 + x\frac{(\mu_L - \mu_G)}{\mu_G}\right]^{-1/4}. \tag{27}$$

4.2 Regime specific models

4.2.1 Separated flow model

In this model the flow of the gas and vapor are analyzed as though the gas and liquid streams flow through separate tubes, with cross-section area proportional to the void fraction. To account for the interaction of the gas and the liquid, appropriate rates of transfer (*e.g.* mass, momentum or energy) are considered in the balance equations in a control volume formulation.

Pressure drop due to flow acceleration
The pressure gradient due to flow acceleration may be written as follows.

$$\left(\frac{dp^*}{dz^*}\right)_{ac} = \frac{d}{dz^*}\left(\frac{1}{A}\int_A \rho u^2 dA\right) = \dot{m}^2 \frac{d}{dz^*}\left(\frac{x^2}{\rho_G \epsilon_{GA}^2} + \frac{(1-x)^2}{\rho_L(1-\epsilon_{GA})^2}\right) \tag{28}$$

Pressure drop due to wall friction
Lockhart-Martinelli correlation
The Lockhart-Martinelli correlation for the two-phase pressure gradient is similar in idea to the two-phase multiplier. A parameter X is defined as

$$X^2 = \frac{(dp^*/dz^*)_{LS}}{(dp^*/dz^*)_{GS}} \tag{29}$$

which is the ratio of the frictional pressure gradients for the liquid and gas alone, flowing at their respective superficial velocities. The single phase pressure drops are obtained using the Fanning equation that uses a friction factor:

$$\frac{dp^*}{dz^*} = \frac{f\rho U^2}{R}, \tag{30}$$

where:

$$f = \frac{16}{Re} \text{ for laminar flow,} \tag{31}$$

and for turbulent flow, two correlations are used:

$$f = \frac{0.079}{Re^{0.25}} \qquad Re \leq 2 \times 10^4, \text{ or} \tag{32}$$

$$f = \frac{0.046}{Re^{0.2}} \qquad Re \geq 2 \times 10^4 \tag{33}$$

where Re is based on pipe diameter i.e. $Re = \frac{\rho UD}{\mu}$, [27].

The two-phase frictional pressure gradient is then obtained by a multiplier defined as

$$\left(\frac{dp^*}{dz^*}\right)_{fr} = \phi_G^2 \left(\frac{dp^*}{dz^*}\right)_{GS} = \phi_L^2 \left(\frac{dp^*}{dz^*}\right)_{LS} \tag{34}$$

$$\phi_G^2 = 1 + CX + X^2 \quad \phi_L^2 = 1 + CX^{-1} + X^{-2} \tag{35}$$

where C is empirically determined and is in the range $5 < C < 20$. The value of C is 5 when the flow of liquid and gas is laminar and 20 when both flows are turbulent.

Friedel correlation

In the Friedel correlation, the two-phase multiplier ϕ_{LO} is calculated differently and the expression for it is given below.

$$\phi_{LO}^2 = E + \frac{3.24FH}{\bar{F}r^{0.045}We^{0.035}} \tag{36}$$

where

$$E = (1-x)^2 + x^2 \left(\frac{\rho_L f_{GO}}{\rho_G f_{LO}}\right)$$

$$F = x^{0.78}(1-x)^{0.24}$$

$$H = \left(\frac{\rho_L}{\rho_G}\right)^{0.91} \left(\frac{\mu_G}{\mu_L}\right)^{0.19} \left(1 - \frac{\mu_G}{\mu_L}\right)^{0.7}$$

$$\bar{F}r = \frac{\dot{m}^2}{2gR\rho_H^2}$$

$$We = \frac{2R\dot{m}^2}{\sigma\rho_H}$$

$$\rho_H \equiv \left(\frac{x}{\rho_G} + \frac{1-x}{\rho_L}\right)^{-1}, \tag{37}$$

and f_{LO}, f_{GO} are the friction factors calculated as if the liquid and the gas respectively were flowing alone in the pipe (see M. M. Awad and Y. S. Muzychka [28], where these parameters are defined).

4.2.2 Pressure drop in bubbly flow

The homogeneous and separated flow models do not consider the regime of the flow in order to predict the pressure drop. One would expect the pressure drop correlations to be tailored to the relevant flow regimes, but such correlations are not generally available.

In the case of bubbly flow in reduced gravity, Colin, Fabre and McQuillen [29] have determined that a friction factor approach correlates the experimentally determined pressure drop quite well. Basically they find that a single-phase Blasius relationship for the friction factor works well when the liquid flow is turbulent.

$$\left(\frac{dp^*}{dz^*}\right)_{bub} = \frac{f_L\rho_L U_L^2}{R}, \quad f_L = 0.079Re_L^{-0.25}, \quad U_L = \frac{U_{LS}}{1-\epsilon}, \quad Re_L = \frac{2\rho_L U_{LS} R}{\mu_L} \tag{38}$$

The predicted pressure drop is quite accurate for Re_L in the range 20,000 to 80,000. For Re_L less than 20,000 the experimentally obtained friction factor is larger than the above prediction. Further, in the case of single phase flow, a sharp increase in the friction factor is observed at a Reynolds number of around 8,000, where there is a transition from a laminar-like behavior to a turbulent-like behavior. Such a behavior is not observed for two phase flow.

4.2.3 Pressure drop in slug flow

Colin, Fabre and McQuillen (1996) [29] comment that for slug flow, the above prediction for bubbly flow shows similar trends when compared to experimental results for slug flow. The data, however display much more scatter. There does not appear to be any other reliable prediction for the pressure drop in slug flow. Bousman [20], who studied exhaustively two-phase flows in microgravity airplane experiments, has found correlations between annular flows pressure drops and the amplitude of waves at the annular interface in the turbulent regime.

In circular channels, there are two possible types of slug flow: one type has continuous liquid phase through the presence of a lubricating liquid layer around each gas bubble (type 1, the kind Bousman observed in his experiments); the other type has completely separate gas-liquid sections down the tube (type 2, [30], discussed below), with sections of wall in contact with either liquid or gas. In square channels, type 2 slug flow cannot exist because there is always liquid in the corners that connects the liquid all along the pipe. In this case, we can have either type 1 when the liquid wholly surrounds each gas bubble, or a hybrid of types 1 and 2 when liquid exists around the bubble only in the corners while the rest of the bubble contacts dry channel wall.

Sang Young Son and Jeff Allen [30] have studied pressure drop in two-phase flow through a square microchannel of 330μm side at relatively low Capillary numbers. The wall was made relatively non-wetting, so that a sequence of gas-liquid volumes can be formed with contact lines, leaving

portions of the tube wall dry. The pressure drop found for this type of slug flow increases as the gas flow rate increases and the flow transitions to "slug-annular" where the gas is completely surrounded by liquid (as in a Bretherton bubble) with contact lines absent. However, a further increase in gas flow rate causes a drastic decrease in pressure drop as the flow transitions to all-annular. This indicates that the extra pressure drop caused in slug flows by the presence of contact lines and/or thin lubricating films around gas bubbles is significant. Alternatively, one could think of this as the effective viscosity of the all-slug flow being higher than that of the all-annular flow for similar flow rates. This is analogous to the well-known fact that the effective viscosity of a foam (i.e., a collection of bubbles separated by very thin liquid layers) is much larger than the viscosity of either of its gas or liquid constituents. For an in-depth study of pressure drop of long bubbles in square channels, see [31, 32, 33].

Other works in pressure drop for two-phase flow in microchannels include Kawahara *et al.* [26] and Triplett *et al.* [34]. Microchannel flow work is important because it may provide information relevant to microgravity. However, one should keep in mind that just scaling the size down does not make a system similar to microgravity. Case in point, bubbly flow is widely documented in microgravity, but it is very difficult to observe bubbly flow (in the sense of having many bubbles across the tube cross section) in microchannels [34].

4.2.4 Comparison of microgravity pressure drop with Lockhart-Martinelli and Friedel predictions

Chen *et al.* (1991) [35] compared several predictions for pressure drop with data for R-114 at various flow qualities. They find that the Lockhart-Martinelli method overpredicts the pressure drop at quality less than 0.6, and underpredicts at higher qualities. The Friedel method consistently underpredicts the pressure drop for almost the entire range of qualities.

Zhao *et al.* (2002) [36] compared measured pressure drop with Lockhart-Martinelli predictions by varying the value of the constant C between 10 and 40, and this band captures most of the measured data. A single value of C, however, fails to represent the data. The same measurements appear to fall in a band of approximately $\pm 40\%$ of the predictions from Friedel's model.

Gabriel (2007) [37] reports that the Lockhart-Martinelli predictions are generally good with an RMS error of 28%. The data also compare very well with Friedel's model with an RMS error of 29%. Curiously, it is stated that Friedel's model generally overestimates the pressure drop. Pressure drop calculations using the homogeneous model are also compared with the experimental data, using both the liquid viscosity and mixture viscosity from Eq. 25 in the model. The overall root-mean-square deviations between the experimental and calculated pressure drop values are 28% when a mixture viscosity is used, and 40% when a liquid viscosity is used.

Narcy and Colin (2015) [38] state that in their experiments the wall shear stress in microgravity (that is related to the pressure drop) is very well predicted by the classical correlation of Lockhart-Martinelli.

4.3 Pressure drop for fully developed, laminar, annular flow

For two-phase flow applications involved in advanced life support, the flow rates are expected to be somewhat low. Therefore, predictions of pressure drop etc., in laminar flow may be an appropriate baseline for such applications. An analysis of fully developed annular flow when the flow is laminar

was performed by Balasubramaniam *et al.* [8]. The analysis reported there also includes the effect of gravity when $\mathbf{g}$ is parallel or antiparallel to the flow.

In fully developed annular flow there are two issues that need to be discussed concerning the structure and stability of the flow. First, there is the issue of which fluid flows next to the wall and which one flows in the center core. In all reduced gravity air-water flows that we are familiar with, water has been reported to be the fluid that is adjacent to the tube wall, and the gas is in the core. It has been suggested that in some two-phase flows a minimum dissipation principle is obeyed, which states that the less viscous fluid occupies the region where the shear stresses are the greatest [39]. In air-water flows, this principle would imply that air is in contact with the tube wall, which appears contrary to experimental observations. Balasubramaniam *et al.* [8] have proposed an argument based on the interfacial energy to develop criteria to determine which phase is in contact with the wall. For most gas-liquid annular flows, the gas is indeed predicted to occupy the core and the liquid is in contact with the wall.

4.3.1 Pressure drop due to wall friction in zero gravity

The results from Balasubramaniam *et al.* [8] specialized for the case of zero gravity shows that the dimensional pressure gradient is

$$\left(\frac{dp^*}{dz^*}\right)_{fr} = \frac{8\mu_L U}{R^2}\frac{M}{h^4(M-1)-M} \tag{39}$$

where $U \equiv (Q_L + Q_G)/\pi R^2$; Q_L, Q_G are the volumetric liquid and gas flow rates, $M = \frac{\mu_G}{\mu_L}$ is the viscosity ratio, and h (h must be less than 1) is obtained from

$$Q_{Gf} = \frac{h^4(2M-1)-2Mh^2}{h^4(M-1)-M} \Rightarrow h = \left[\frac{[M(Q_{Gf}-1)\{M(Q_{Gf}-1)-Q_{Gf}\}]^{1/2}-M}{1+M(Q_{Gf}-2)-Q_{Gf}}\right]^{1/2} \tag{40}$$

where Q_{Gf} is the gas volume flow fraction. The physical thickness of the liquid film adjacent to the tube wall is $R(1-h)$.

4.3.2 Pressure drop due to flow acceleration

Flow acceleration occurs when the flow is developing, such as in entrance flows, or if there is a change in the flow geometry, such as when the flow encounters an expansion, contraction, or a bend. Flow acceleration can also be caused by phase change, see for example [7]. In the case of fully developed flow, there is no flow acceleration. Therefore, strictly speaking, the pressure drop due to flow acceleration is zero. One might, however, approximate the flow to be locally fully developed, with variations in z occurring over a much longer length scale than the length of pipe required to achieve fully developed flow. Using such an assumption, the pressure drop due to flow acceleration may be written as follows.

$$\left(\frac{dp^*}{dz^*}\right)_{ac} = \frac{d}{dz^*}\left(\frac{1}{A}\int_A \rho u^2 dA\right) \tag{41}$$

In eq. 41 all variables are dimensional. Using the pseudo velocity scale $w_{ps} = Q/\pi R^2$, and the pseudo length scale R,[2] we find

[2]We use the term "pseudo scale" to indicate that the scale is not a constant quantity but is a function of z through $R = \mathcal{R}(z)$.

$$\left(\frac{dp^*}{dz^*}\right)_{ac} = \frac{-8Q^2}{\pi^2\mu_L R^5}\frac{dR}{dz^*}\left[\rho_L\int_h^1 w_L^2 r dr + \rho_G\int_0^h w_G^2 r dr\right]. \tag{42}$$

$$w_L = \left(\frac{2M}{h^4(M-1)-M}\right)(r^2-1) \tag{43}$$

$$w_G = \left(\frac{2M}{h^4(M-1)-M}\right)\left[h^2\left(1-\frac{1}{M}\right)-1+\frac{r^2}{M}\right] \tag{44}$$

$$\left(\frac{dp^*}{dz^*}\right)_{ac} = - \frac{16\frac{dR}{dz^*}M^2Q^2\left(\frac{h^6\rho_G}{M^2}+3h^2\rho_G\left(h^2\left(1-\frac{1}{M}\right)-1\right)^2-\left(h^2-1\right)^3\rho_L+\frac{3h^4\rho_G\left(h^2\left(1-\frac{1}{M}\right)-1\right)}{M}\right)}{3\pi^2\mu_L R^5\left(h^4(M-1)-M\right)^2} \tag{45}$$

5 Heat transfer in reduced gravity two phase flows

5.1 Single phase flow

In single fluid flow analyses, the relationship between wall heat transfer and wall friction has been exploited routinely to develop expressions for heat transfer coefficients from the friction factor data. For fully developed turbulent flow in a pipe with molecular and turbulent Prandtl numbers close to unity ($Pr = \frac{\nu}{\alpha}$, where $\nu = \mu/\rho$ is kinematic viscosity, and $\alpha = k/\rho\, c_p$ is thermal diffusivity), the assumption that heat and momentum are transported at the same rate produces the following relationship between the thermal and flow fields:

$$\frac{q^*}{c_p\tau^*}du = dT, \tag{46}$$

where q^* is heat flux normal to the wall and τ is shear stress. If, in addition, it is further assumed that the ratio of heat flux to shear stress is constant across the domain such that

$$\frac{q^*}{\tau^*} = \frac{q^*_W}{\tau^*_W},$$

where the subscript W denotes the quantity evaluated at the tube wall, eq. 46 can be integrated between the wall and mean bulk conditions to provide the following relationship between wall heat flux and shear stress:

$$\frac{q^*_W u_m}{\tau^*_W c_p} = T_W - T_b. \tag{47}$$

Here u_m and T_b are the flow velocity and temperature outside the boundary layer respectively. When the definitions of heat transfer coefficient, $q^* = \tilde{h}(T_W - T_b)$, and Fanning friction factor,

$\tau_W^* = \frac{f}{2}\rho u_m^2$ are substituted into eq. 47, a relationship between wall heat transfer and Fanning friction factor is derived:

$$St = \frac{f}{2}. \tag{48}$$

Here the Stanton number, St, represents the ratio of wall to convective heat transfer given by:

$$St \equiv \frac{\tilde{h}}{\rho c_p u_m}.$$

Equation 48 is called the Reynolds analogy for pipe flow and strictly speaking is only valid for fully developed turbulent pipe flows with molecular and turbulent Prandtl numbers equal to one [40]. A similar relationship between wall friction factor and heat transfer coefficient can be derived for turbulent and laminar boundary layer flows over a flat plate. This relationship is also known as the Colburn analogy [40]:

$$St\ Pr^{2/3} = \frac{f}{2}. \tag{49}$$

Colburn's analogy suggests that there is a Prandtl number dependence of $Pr^{2/3}$ for the flat plate problem. Curiously, it turns out this dependence also works well for turbulent pipe flows. Thus for turbulent pipe flows, a Reynolds analogy can be written that includes the Prandtl number dependence of the fluid in the form of eq. 49.

Even for single phase flows, one has to be cautioned that, while the friction-heat-transfer analogies can be applied to both laminar and turbulent flows over a flat plate and to turbulent pipe flows, they are not valid for laminar pipe flows and that, in general, more rigorous treatments of the governing equations and boundary conditions are needed when seeking new applications for these analogies. Specifically, Knudsen and Katz [41] have shown that for more generalized applications of the heat-transfer-fluid-friction analogies, the resulting expressions often do not take the simple forms represented by eq. 49.

The result in Eq(49) can also be cast as an expression for the Nusselt number. Using $f = 0.046Re^{-0.2}$ for turbulent flow, the Nusselt number is

$$Nu = Re\ Pr\ St = \frac{f}{2} Re\ Pr^{1/3} = 0.023 Re^{0.8} Pr^{1/3} \tag{50}$$

A similar correlation has been provided by Dittus and Boelter, who write

$$Nu = 0.023 Re^{0.8} Pr^{n} \tag{51}$$

where $n = 0.4$ when the fluid is heated and $n = 0.3$ if it is cooled. When viscosity variation in the cross section is important, the Sieder-Tate correlation is used.

$$Nu = 0.023 Re^{0.8} Pr^{1/3} \left(\frac{\mu_b}{\mu_w}\right)^{0.14} \tag{52}$$

where μ_b is the bulk fluid viscosity and μ_w is the fluid viscosity at the wall.

5.2 Two phase flow without phase change

For two-phase flow of a liquid and gas without phase change, or for two phase flow of a liquid with only a small amount of phase change, the Reynolds or Colburn analogy (Eq 49) can be used to determine the heat transfer coefficient where the property values are evaluated for two-phase conditions.

5.2.1 Homogeneous flow

For the homogeneous flow model, we can use Eq(50) with the Reynolds number computed as $Re = \frac{4\dot{M}}{\pi D \mu_H}$, where the effective viscosity for homogeneous flow μ_H can be calculated from Eqs. 22 to 25 as appropriate.

$$Nu = 0.023 \left(\frac{4\dot{M}}{\pi D \left[x\mu_G + (1-x)\mu_L \right]} \right)^{0.8} Pr^{1/3} \tag{53}$$

5.2.2 Annular flow

For annular flow, the two phase properties are evaluated using the separated flow model. The Nusselt number can be written as

$$Nu = \frac{1}{2} f_{lo} \phi_l^2 \frac{\rho_H}{\rho_L} (1-x)^2 Re\ Pr^{1/3} \tag{54}$$

where the friction factor multiplier is $\phi_l^2 = 1 + \frac{C}{X} + \frac{1}{X^2}$, with C a constant that depends on the nature of the liquid and vapor flow, $X = \frac{(dp/dz)_l}{(dp/dz)_g}$ is the Lockhart-Martinelli parameter, $\left(\frac{dp}{dz}\right)_l = \frac{2 f_l \dot{m}^2 (1-x)^2}{\rho_L D}$, $\left(\frac{dp}{dz}\right)_g = \frac{2 f_g \dot{m}^2 x^2}{\rho_G D}$, where f_l and f_g are the liquid and gas friction factors. Chisholm [42] recommends $C_{tt} = 20$ for turbulent liquid and gas flow, $C_{vt} = 12$ for laminar liquid and turbulent gas flow, $C_{tv} = 10$ for turbulent liquid and laminar gas flow, $C_{vv} = 5$ for laminar liquid and gas flow.

Balasubramaniam *et al.* (2006) have analyzed fully developed annular flow with heat addition in a tube when the flow is laminar. The effect of gravity that is oriented parallel to the tube axis was included in the analysis. Specializing their analysis for zero gravity, the results for the flow are given in Eqs. (39) to (45), and the Nusselt number is given below.

$$Nu = \frac{\text{num}}{\text{den}} \tag{55}$$

$$\text{num} = -48\beta \left\{ \rho_G C_{p_G} h^2 \left[h^2(2M-1) - 2M \right] - \rho_L C_{p_L} M \left(h^2 - 1 \right)^2 \right\}^2$$

$$\begin{aligned} \text{den} = &-\rho_G^2 C_{p_G}^2 h^4 \left[h^4(24M^2 - 32M + 11) + 16h^2 M(2-3M) + 24M^2 \right] + \\ &12\beta C_{p_G} C_{p_L} \rho_G \rho_L M h^2 (h^4 - 4h^2 + 3) \left[h^2(2M-1) - 2M \right] + \\ &24\beta h^4 \ln h \left\{ \rho_G C_{p_G} \left[h^2(2M-1) - 2M \right] - \rho_L C_{p_L} M (h^2 - 2) \right\}^2 + \\ &\beta \rho_L^2 C_{p_L}^2 M^2 (-9h^8 + 56h^6 - 108h^4 + 72h^2 - 11), \end{aligned}$$

where $\beta \equiv \frac{k_G}{k_L}$, the ratio of gas to liquid thermal conductivity. For air and water, $\beta = 0.041$.

For air and water, with water wetting the tube wall, the variation of the Nusselt number with scaled

radial location of the liquid film h is shown below. The values at $h = 0$ and 1 are $\frac{48}{11}$ and $\frac{48\beta}{11}$, respectively. The Nusselt number is a maximum for a liquid film that has a thickness of approximately 20% of the tube radius.

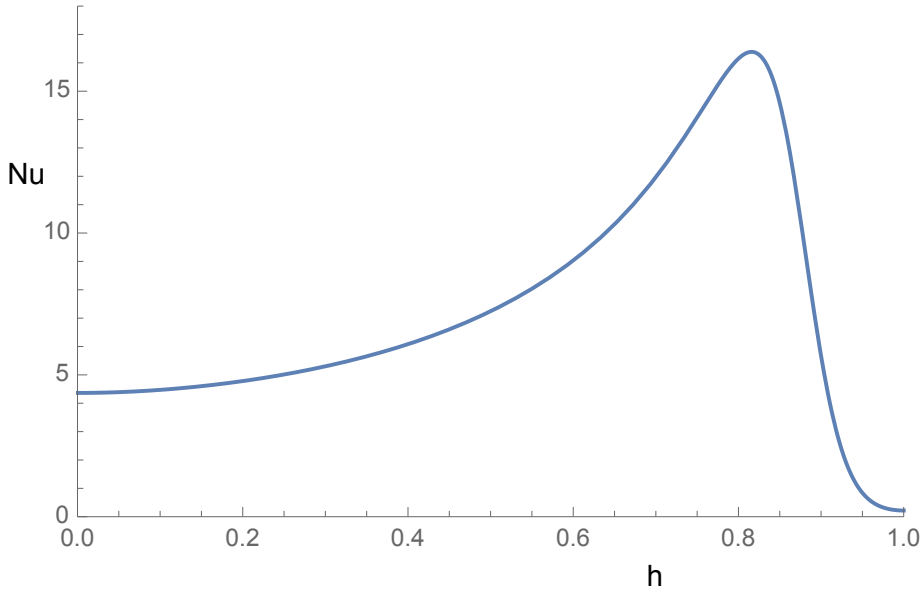

Figure 2: Nusselt number for air-water in laminar annular flow versus radial position of the gas-liquid boundary, h. Water flows along the wall; air flows in the tube center. $\beta = 0.048$.

5.3 Flow with phase change

The two-phase flow of a liquid with phase change due to heat addition on the tube wall has several flow regimes as the flow moves downstream. Starting with subcooled, liquid only flow near the entrance region, the flow progress through a subcooled boiling region where bubbly flow occurs, followed by a saturated boiling region where bubbly flow transforms to slug flow. After saturated boiling, heat transfer occurs via evaporation in a thin annular liquid film where the flow is annular. Forced convection heat transfer in the film is predominant, and boiling is suppressed. At the end of this region, the liquid film at the wall is dried up, and the flow is essentially a vapor flow, with some entrained drops. Beyond the region where the liquid film is absent, the rate of heat transfer diminishes significantly.

A significant issue for heat transfer with phase change is the critical heat flux – the maximum heat flux that can be achieved. For efficient heat transfer, liquid must contact the wall where heat is added. If the wall is blanketed by a vapor layer, then heat must be transferred through this layer to reach the liquid, and the heat transfer is not effective. After critical heat flux, there is transition boiling whereby as the temperature increases, the heat flux decreases. Dryout and then burnout is the final step. Also, for many fluids, the wall temperature rises sharply beyond the critical heat flux to support the given heat load. All practical systems using boiling usually operate below the critical heat flux. The critical heat flux depends on the g-level. For both pool boiling and flow boiling, the critical heat flux under microgravity is currently being researched. Generally the critical heat flux is larger for flow boiling than pool boiling, and increases with the flow speed. Hall and Mudawar [43] have developed a statistical correlation for the critical heat flux based on water data in normal

gravity, and has been found to apply for other fluids as well.

$$Bo = \frac{C_1 Wb^{C_2} \left(\rho_L/\rho_G\right)^{C_3} \left(1 - C_4 \left(\rho_L \rho_G\right)^{C_5} x_{eq,in}\right)}{1 + 4C_1 C_4 Wb^{C_2} \left(\rho_L/\rho_G\right)^{C_3+C_5} \left(L/D\right)} \tag{56}$$

where $Bo = \frac{q_c}{\dot{m} h_{fg}}$, q_c is the critical heat flux, $Wb = \frac{\dot{m}^2 D}{\rho_L \sigma}$, $x_{eq,in} = [h(T_{in}, P_{in}) - h(T_{sat}, P_{in})]/h_{fg}$ is the equilibrium inlet quality, $C_1 = 0.0722$, $C_2 = -0.312$, $C_3 = -0.644$, $C_4 = 0.9$, and $C_5 = 0.724$.

We present two heat transfer correlations by Chen [44] and Kim and Mudawar [45] for flow with phase change. Both correlations represent the total heat transfer as a combination of that due to nucleate boiling and forced convection.

5.3.1 Chen correlation

The Chen correlation [44] calculates the total heat transfer coefficient as a superposition of the nucleate boiling and forced convection heat transfer coefficients. The nucleate boiling heat transfer is multiplied by a suppression factor to incorporate the suppression of boiling in the annular flow regime. The forced convection heat transfer in single phase (liquid only) is augmented by an enhancement factor, which is a two-phase multiplier. The heat transfer coefficient is written as

$$h = S\, h_{nb} + E\, h_l \tag{57}$$

$$h_l = 0.023 \frac{k_L}{D} Re_L^{0.8} Pr^{0.4} \tag{58}$$

$$h_{nb} = 0.00122 \left[\frac{k_L^{0.79} C_{p_L}^{0.45} \rho_L^{0.49}}{\sigma^{0.5} \mu_L^{0.29} h_{fg}^{0.24} \rho_V^{0.24}}\right] (T_w - T_{sat})^{0.24} (P - P_{sat})^{0.75} \tag{59}$$

$$E = \left(1 + \frac{1}{X_{tt}}\right)^{1.78} \tag{60}$$

$$S = 0.9622 - 0.5822\ \tan^{-1}\left(\frac{Re_L\, E^{1.25}}{6.18 \times 10^4}\right) \tag{61}$$

$$X_{tt} = \left(\frac{\mu_L}{\mu_G}\right)^{0.1} \left(\frac{1-x}{x}\right)^{0.9} \left(\frac{\rho_G}{\rho_L}\right)^{0.5} \tag{62}$$

where $Re_L = \frac{\dot{m}(1-x)}{\rho_L}$ and x is the thermodynamic vapor quality. Note that since the liquid to vapor density ratio large, even a small value of x ($x \sim 0.1$) can cause the void fraction to be large ($\alpha \sim 0.9$ when the density ratio is 100 and the liquid and vapor velocities are comparable), thus promoting annular flow. The relationship between the area based void fraction α, the slip ratio $S = \frac{V_v}{V_l}$, and the thermodynamic quality may be obtained as

$$\alpha = \frac{A_v}{A_v + A_l} = \frac{1}{1 + S \frac{\rho_V}{\rho_L} \frac{(1-x)}{x}}. \tag{63}$$

5.3.2 Kim and Mudawar correlation

In the Kim and Mudawar [45] correlation, the heat transfer coefficients for nucleate boiling, convective boiling and total heat transfer are calculated differently.

$$h = \left(h_{nb}^2 + h_{cb}^2\right)^{0.5} \tag{64}$$

$$h_{nb} = \left[2345\left(Bo\frac{P_h}{P_w}\right)^{0.7} P_R^{0.38}(1-x)^{-0.51}\right]\left(0.023\frac{k_L}{D}Re_L^{0.8}Pr^{0.4}\right) \tag{65}$$

$$h_{cb} = \left[5.2\left(Bo\frac{P_h}{P_w}\right)^{0.08} Wb_{lo}^{-0.54} + 3.5\left(\frac{1}{X_{tt}}\right)^{0.94}\left(\frac{\rho_G}{\rho_L}\right)^{0.25}\right]\left(0.023\frac{k_L}{D}Re_L^{0.8}Pr^{0.4}\right) \tag{66}$$

where $Bo = \frac{q}{\dot{m}h_{fg}}$, $P_R = \frac{P}{P_{crit}}$, $Wb_{lo} = \frac{\dot{m}^2 D}{\sigma\rho_L}$, and P_h and P_w are the heated and wetted perimeters in the tube.

In both the Chen [44] and Kim and Mudawar [45] correlations, the vapor quality x, and therefore the liquid Reynolds number, depend on the axial location in the tube. If x changes appreciably, calculations must be performed for several short tube length segments (Δz) over the entire length of the tube, so that the change in x in each axial segment can be regarded as constant.

5.3.3 Heat transfer correlation for condensation in tubes

Shah (1979) provided the following correlation for condensation in tubes.

$$h = \left(0.023\frac{k_L}{D}Re_L^{0.8}Pr^{0.4}\right)\left[(1-x)^{0.8} + \frac{3.8\,x^{0.76}(1-x)^{0.04}}{P_R^{0.38}}\right] \tag{67}$$

where x is the local vapor quality and P_R is the reduced pressure (operating pressure divided by the fluid's critical pressure). This correlation, developed for normal gravity applications, does not depend on the nature of the flow regime in the tube, or tube orientation. Recently, the author (Shah 2009) has improved and extended his original correlation to lower flow rates, tested it for many new refrigerants for all tube orientations with respect to the gravity vector, and wider operating pressures. Kim and Mudawar [45] also provide heat transfer correlations for condensation in tubes that depend on the nature of the flow regime. The correlation given above appears to perform fairly well for a wide range of conditions.

Since gravity does not appear explicitly in this correlation, it may be useful to calculate a baseline heat transfer correlation for microgravity using eq. 67. However, this needs to be verified and is a topic of current research.

5.3.4 Validity of flow boiling heat transfer correlations in low gravity

The heat transfer correlations given above have all been developed for use in normal gravity. Narcy and Colin (2015) [38] have reviewed heat transfer in flow boiling in reduced gravity. Based on results of studies conducted since 2003, they state that the low quality subcooled nucleate boiling regime, that exhibits bubbly and slug flows, is sensitive to gravity at low mass flux (i.e., mass flow rate per unit cross sectional area). When the mass flux is high, the effect of gravity disappears. When

the vapor quality is high, the rate of heat transfer is generally unaffected by gravity. When the mass flux and vapor quality are high, annular flow without nucleate boiling prevails, and the heat transfer coefficient is predominantly due to forced convection liquid film evaporation. The exception is at very low mass flux where nucleate boiling in the annular flow regime occurs; here the heat transfer coefficient is reduced compared with that in normal gravity. To our knowledge, correlations where low gravity has a significant effect on the heat transfer are yet to be developed and tested.

6 Two phase flow through specific components

6.1 Bends, tees, expansion and contraction

6.1.1 Bends

When a flow moves through a bend, it is subjected to a centrifugal force as the fluid elements undergo rotation to conform to the geometry of the bend. In a two-phase flow, the centrifugal force would tend to move the gas towards the axis of the bend (the inner surfaces of the tube closer to the center of the bend), and the liquid away from the axis. However, secondary forces due to viscous effects also occur that tend to move liquid towards the inner surface. Experiments in normal gravity in helically coiled tubes with annular flow have observed both instances of liquid at inner and outer tube wall depending on liquid and gas flow rates (Hart *et al.* [46]). Flow in a single bend, however, is likely to be different from that in a helically coiled tube, but the same forces are at work. The behavior of such flows in microgravity has not been studied, to our knowledge.

For bubbly flows, centrifugal forces would tend to move bubbles to the inner wall as well. Koch and Sangani [47] predict that bubble-phase pressures arising from bubble interactions would tend to move bubbles towards regions in the liquid where there are less bubbles, and compete with the centrifugal force. Microgravity tests to demonstrate these expectations have not been performed, to our knowledge.

6.1.2 Expansions

Bubbly and slug flows of air-water system in reduced gravity readily conform to the larger diameter tube after expansion for low flow rates (McQuillen and Motil [48]). Usually there is a recirculation zone or a gas pocket in the corner of the expansion tube. At high flow rates, a two-phase jet develops after expansion when the flow enters an initially dry tube. Cylindrical (Taylor) bubbles, if present, expand radially and contract axially and tend to a more spherical shape. Their rupture and interaction with the wall is quite complex leading to break-up of the jet and deposition of liquid on the wall.

6.1.3 Contractions

Tests by McQuillen & Motil [48] revealed several features of two phase flow through contractions. Transition from bubbly flow to slug flow occurs for large bubbles with a diameter greater than the contracted tube diameter, as they are radially compressed. An important observation is that slug flow does not seem to result from coalescence of small bubbles. In some cases, the liquid film at the mouth of the contraction dries out, and results in the formation of a gas pocket there. The behavior of Taylor bubbles entering the contraction is interesting. A liquid bridge forms at the contraction but is unstable and collapses downstream. If two Taylor bubbles enter the contraction, and are separated by less than one tube diameter, the liquid between the bubbles drains, and the bubbles coalesce.

6.1.4 Tees

Low gravity aircraft tests by Jayawardena and McQuillen [49] show that it is very difficult for liquid to turn a corner and flow down the side arm at a tee-junction. The amount of liquid flowing through the sidearm was 20-50% of the inlet flow, for all types of flow patterns in the inlet tube. In normal gravity Yang *et al.* [50] have used a multi-tube tee junction and show that with five or more connecting tubes, a multi-tube junction can lead to complete separation of air and water. Similar tests do not appear to have been performed in reduced gravity.

6.2 Separator

Even in reduced or in zero-gravity, processes require the separation of two immiscible phases. Separation is hindered by the absence of a natural buoyant force, which drives density segregation in gravitational environments. In this section we will discuss several phase separation methods. In the first one, the 2-phase mixture is forced into a cyclonic chamber where the centripetal acceleration replaces the gravitational acceleration. In the second one, the separation is driven by geometry and capillary flow. The third method uses a hydrophobic membrane placed at the wall of the flow channel to extract gas bubbles. Finally, we describe a syringe-based method using a screen or a perforated disc to remove bubbles from a small liquid sample. Each separation method operates optimally in very different ranges of flow rate.

6.2.1 Centrifugal cyclonic separator

This method works well for relatively high gas and liquid flow rates, even though it is possible to use cyclonic separators with rather low flow rates in zero gravity [51, 52, 53, 54]. These separators consist of a cylindrical container of radius R, with an injection port in the side wall where the 2-phase mixture enters tangentially and with a purely angular velocity; refer to fig. 3. The 2-phase mixture self organizes into a swirl motion. The lighter phase (usually gas) migrates to the center by centripetal buoyancy, while the heavier phase (usually liquid) is pushed against the wall. Under proper operating conditions, a gas core of radius R_c forms in the center, so the gas may is tapped from an outlet orifice on the 'top' end plate. The liquid that flows into the space between the baffle plate and the bottom end plate is essentially gas-free, and is withdrawn from an orifice in the bottom plate.

Design of these devices must consider the characteristic times for a bubble flight into the gas center core by buoyancy, t_r, and that for the flow to traverse the distance between the top plate and the baffle plate, t_z. Since the amount of gas in the liquid outlet decreases as the ratio t_r/t_z decreases, good design must ensure that $t_r/t_z \ll 1$ under all the flow combinations in the operating envelope [52].

The limits of operation are set by two types of flow condition: 1) flow rate combinations that cause the swirl layer thickness, $R - R_c$, to be less than the baffle plate-wall gap, $R - R_{\text{baff}}$ (implying that $R_c > R_{\text{baff}}$), as this condition will allow gas in the liquid outlet; and 2) flow rate combinations that make $R_c = 0$, thus flooding the gas exit port. In general, for fixed liquid flow rate increasing the gas flow rate increases R_c and vice-versa. And, for fixed gas flow rate, increasing liquid flow rate decreases R_c and vice-versa.

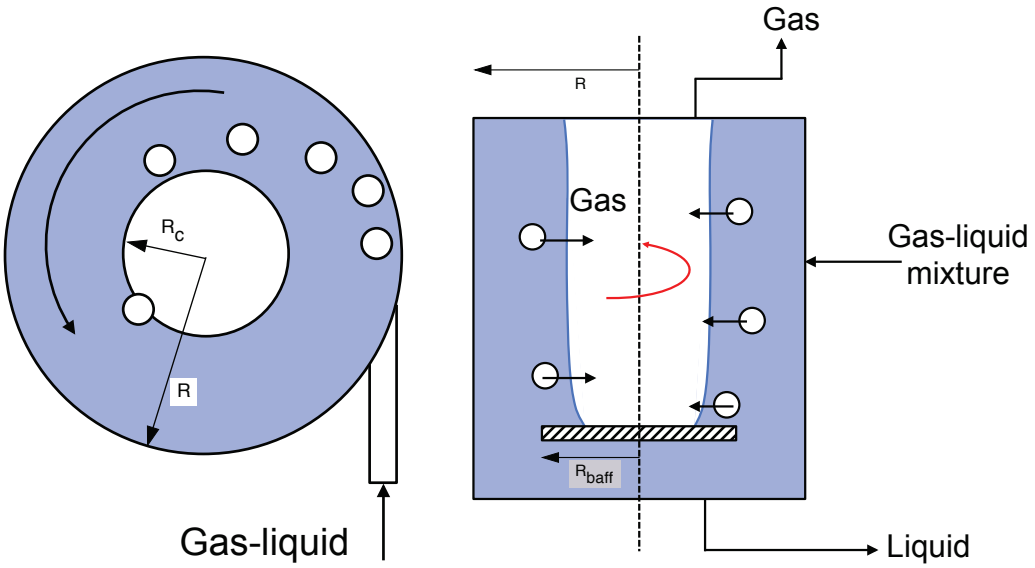

Figure 3: Schematic of a cyclonic separator. Left: top view. Gas –depicted as bubbles dispersed in the liquid, is shown in white; liquid is shown in light blue. The gas center core exists between the top end plate and a circular baffle plate. Virtually gas-free liquid is tapped under the baffle plate through an orifice in the bottom end plate.

6.2.2 Capillary flow separation

Capillary-flow-driven separation is appropriate for relatively small gas and liquid flow rates. This form of phase separation exploits the flow that arises in a corner channel in the presence of a non-spherical bubble, see fig. 4 [55, 56]. If the bubble volume is larger than the maximum bubble that can exist as a sphere in the channel, it is clear than some portion of the bubble surface will rest on the channel walls as seen in the figure, creating either a dry solid area, or a thin liquid film between the gas and the channel wall. The rest of the bubble surface forms a meniscus between the channel walls. Due to the V-shape in the channel cross-section, the curvature of the bubble surface is not constant, being larger near the corner of the V-channel ($\sim 1/R_1$) and smaller away from the corner ($\sim 1/R_2$). Since a static situation can only exist when the bubble curvature is constant, it follows that this configuration must have a flow associated with it. In fact, based on the curvatures just discussed, liquid is driven to the space between the corner and the bubble, thus forcing the bubble to move away from the corner and towards the liquid-air interface.

Since the migration velocity of the bubble perpendicularly away from the corner can be estimated [56], design of a corner channel separator can yield the time for the bubble to burst through the interface between the liquid and the ambient air as it moves from an initial position towards the interface. Often, though, these channels are used with imposed flow along the corner. In this case, the length of channel required for all the bubbles to burst through the liquid-air interface is the critical design calculation and can be achieved using the estimates of migration velocity away from the corner.

6.2.3 Membrane separation

As fig. 5 shows, this method uses a hydrophobic membrane, placed on the flow channel wall, to remove bubbles in a gas-liquid flow. The method has been demonstrated for flows in sub-millimeter

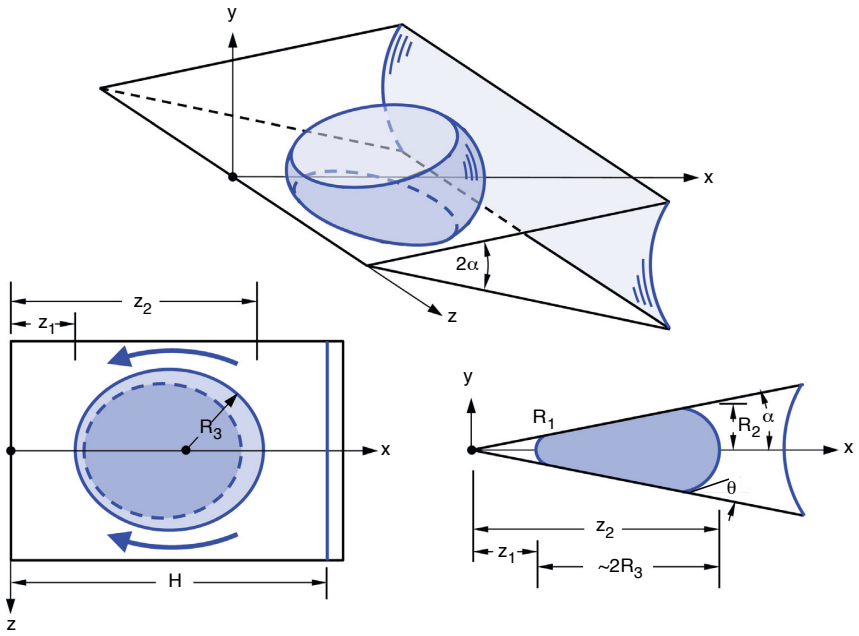

Figure 4: Schematic of a confined bubble in a wedge of angle 2α. Top: Isometric view. Bottom left: view down the y axis. Bottom right: cross section through bubble center. R_3 is the characteristic radius of curvature in the x-z plane. R_1 and R_2 are the respective characteristic radii of curvature at the narrowest and widest parts of the bubble (after Weislogel [56]).

channels, although it should be possible to explore scaleup rules. A bubble, larger than the channel width H, travels in a liquid stream. When the bubble encounters the membrane-covered wall, the pressure in the other side of the membrane sucks the gas out of the liquid [57]. Other designs that incorporate hydrophilic and hydrophobic materials are possible, see `https://medical.pall.com/en/pall-solution/posidyne--eld-filter.html`.

Five criteria must be satisfied for this method to work:

1) Bubble size (defined as the radius of a sphere having the same volume as the bubble) must be larger than channel width H. This ensures that the gas will contact the membrane.

2) Bubble travel time over membrane $>$ time for membrane to absorb all gas in bubble. The bubble travel time is a function of the average velocity in the channel. The extraction time depends on the flow rate of gas through the membrane, Q which can be estimated using Darcy's law, $Q = A\kappa\Delta p/(\delta\mu_G)$ knowing the membrane thickness and permeability, δ and κ, the gas viscosity μ_G, the gas-membrane contact area A, and the pressure difference across the membrane.

3) The velocity of the leading contact line moving along the membrane (the contact line of the receding liquid) must be less than the critical velocity to deposit a Landau-Levich liquid film layer on the solid. This ensures that the contact area of the bubble on the membrane remains dry, thus allowing gas extraction. For a system with static contact angle θ_0, the critical velocity for film deposition is approximately $u_c \approx \theta_0^3\sigma/36\mu$. The coefficient 36 depends weakly on velocity and on macroscopic length scale. The more hydrophobic the surface, the larger θ_0 and the higher the critical velocity for liquid layer deposition.

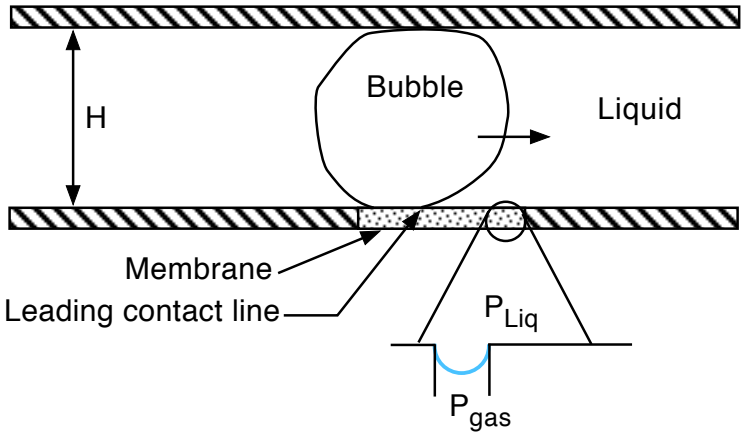

Figure 5: Schematic of a gas bubble passing by a membrane installed in the channel wall. The zoom-in schematic shows the membrane covered by liquid, and sustaining a pressure difference $P_{\text{Liq}} - P_{\text{gas}}$ by capillarity. For a liquid-gas system with surface tension σ, the maximum pressure difference that a membrane with pore radius R_p can sustain without allowing liquid through is $2\sigma/R_p$.

4) Given a membrane with typical pore radius R_p, the pressure difference across the membrane must be less than maximum pressure drop above which liquid breaks through: $P_{\text{Liq}} - P_{\text{gas}} < 2\sigma/R_p$. The reason for this criterion is obvious: it guarantees that only gas flows through the membrane.

5) Membranes must not be fouled by particulate matter or chemicals that can alter their wettability.

6.2.4 Removal of bubbles from a small liquid volume

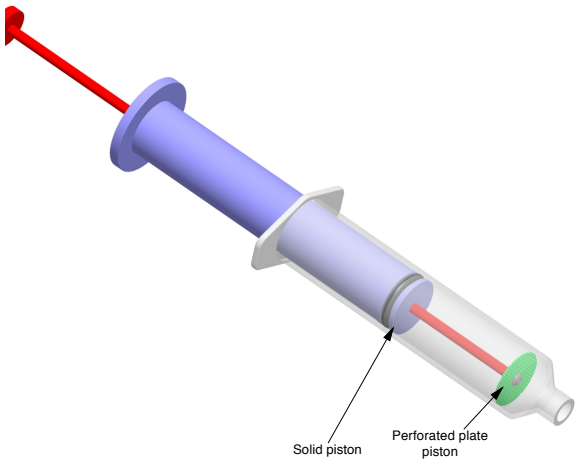

Figure 6: Schematic of the dual-piston syringe.

In several small scale applications in microgravity, there is a need to produce a small volume of bubble-free liquid, or render a small amount of bubble-laden liquid to be free of gas. A few examples are (i) coffee cup or drink pouch, where astronauts typically consume the liquid by sipping in the manner they do in normal gravity. The drink pouches are designed with sharp corners, so that

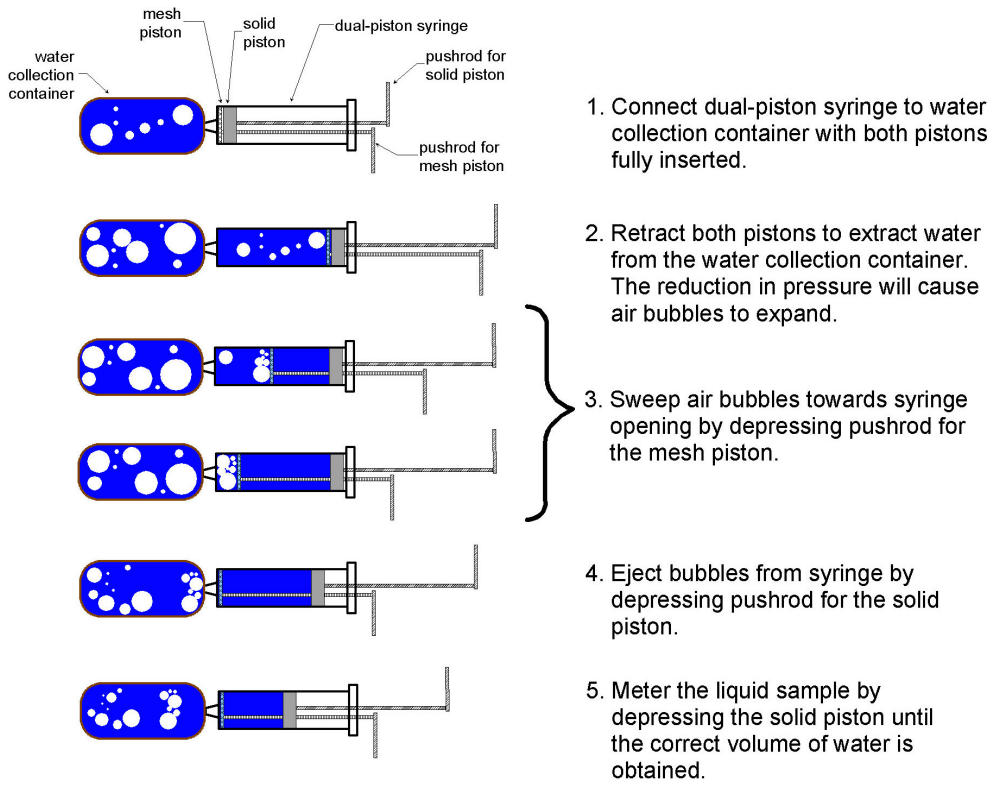

Figure 7: Removal of gas bubbles for a small liquid volume.

liquid is naturally entrained in the region near the corner, with any bubbles that are present being forced away as discussed in Section 6.2.2. (ii) generation of intravenous injection fluids, starting with distilled water and crystalline salts. The IVGEN experiment (McQuillen *et al.* [58]) attempted to produce IV fluids on orbit, utilizing ISS water that was deionized. The water was mixed with salt in an IV bag. The amount of water must be precisely controlled so that the concentration of the saline solution falls within an allowable range (5%) of the required value. The IVGEN experiment did encounter problems with an inaccurate estimate of the volume of the transfer line from the ISS water supply to the accumulator. (iii) measurement of water quality, to ensure that there are no contaminants in ISS potable water and the amount of iodine, colloidal silver, etc. that are added as biocides to the water are within specifications. Dias, Porter and Fritz [59] mention that their early experiments on water quality assessments for iodine had challenges associated with removal of air bubbles entrapped in a water sample in KC-135 aircraft microgravity tests, precluding the precise measurement of water sample volume. The volume measurement was crucial for the technique they initially used, after which they attempted to develop methods that are insensitive to the precise sample volume.

At NASA GRC, we have developed a syringe based method to remove bubbles from a small volume of liquid. The concept consists of a syringe with a dual plunger and is illustrated in fig. 6. The operation procedure is summarized in fig. 7. Basically the syringe is outfitted with a second plunger that operates a mesh/screen or a perforated plate. The syringe with both pistons pushed all the way in is connected to the liquid source which contains some gas. The two pistons retreat, taking in a liquid sample, along with the gas. The perforated plate piston is pushed toward the exit, sweeping the gas ahead of the plate in the process.. While liquid flows freely through the perforated disc, it is

designed so that air bubbles do not penetrate it. Once the bubbles are concentrated near the syringe exit, they coalesce, thus draining all the inter-bubble liquid. At this point, the solid piston is pushed, causing the gas to exit the syringe, rendering the liquid sample in the syringe to be bubble free. The device has not been tested in microgravity, but works under all orientations in normal gravity.

It should be pointed out that a screen or mesh based device is used in other applications in low gravity, for example Liquid Acquisition Devices (LAD) in propulsion fuel tanks, where there is a need to acquire and transport fuel from storage tanks to the engine, without ingesting vapor. The screen is placed in the tank near a wall and isolates the liquid from the gas phase by inhibiting gas penetration into the liquid on account of its high bubble point pressure.

6.2.5 Moving unwanted bubbles in systems

Moving gas bubbles in liquids in low gravity is not easy. On Earth we take it for granted that gas bubbles move to the top of a liquid, for example when we pour a carbonated beverage in a container. Without buoyancy, bubbles would stay in place in a liquid as there is no force to move them.

Free bubbles in a liquid can be carried away by a liquid flow. An adequate flow would be necessary to dislodge and move bubbles stuck to walls. Bubbles at rest in a liquid can in principle be moved by creating a variation in the surface tension along the liquid/gas interface. For example, by heating the liquid on one side, a variation in temperature and consequently surface tension can be created on the bubble surface. The thermocapillary stress generated (Subramanian and Balasubramaniam [60]) would move the bubble from cold to hot regions in a liquid. In practice, a hot spot might be created on a wall, and the gas could be sucked away through a port when the bubble is in its vicinity. Note that anytime gas is removed from liquid, a corresponding amount of pure liquid must be supplied back for volume compensation. In principle, the thermocapillary mechanism should work even if the bubble is in contact with a solid wall. Unfortunately, when the liquid is water, the water/air interface (or that with another gas) is very susceptible to be contaminated with minute amounts of surface active substances that affect the surface tension, and the thermocapillary mechanism as a means to manipulate bubbles invariably fails.

An alternative way of moving unwanted bubbles is by using the capillary force and the dynamics of contact lines. This would not work, however, for bubbles fully submerged in liquids. The idea is to manipulate the contact line between solid, liquid and gas by means of suitably designed wall wettability properties and/or flow cross sections (sharp corners, etc.) so that contact lines can be moved to desired locations that are predetermined. A port near these areas would be used to suck the gas away.

Other methods to manipulate bubbles include the use of acoustic and electromagnetic means, but have not been rigorously tested for low gravity applications. The above discussion is to underscore the message that moving and removal of unwanted bubbles in microgravity is difficult and tedious. It behooves the designer to think in advance about possible sources of bubble production and introduction in critical locations in the system and prevent such occurrences.

6.3 Filter

Filters are used to remove particulate matter from a liquid or gas. In low gravity they should work as they do in normal gravity and terrestrial design experience will be adequate. What needs to be filtered, however, might not be intuitive in low gravity. For example, in the context of the removal

of CO_2 using the Carbon Dioxide Removal Assembly (CDRA) on the ISS using a packed bed of zeolite, fine particles of zeolite material were escaping the bed assembly and depositing in key components downstream. This necessitated a redesign as well as the addition of inline filters to the unit on orbit (El Sherif and Knox [61].).

6.4 Pumps

It is well known that pumping liquid that contains gas is problematic for the commonly used centrifugal (or rotodynamic) pumps. The efficiency and pump head decrease when gas is ingested by the pump. When the gas flow fraction exceeds a limit (typically around 10%) the pump loses prime and the ability to flow liquid. Basically the impeller within the pump acts as a separator for gas and liquid, with the gas accumulating at the center of the impeller. If sufficient amount of gas accumulates, the vane passages in the pump are filled by gas, blocking the liquid flow.

Two-phase pumps have primarily been developed for applications in the oil industry (see for example Hua *et al.* [62]; Khalili *et al.* [63]; Cooper *et al.* [64]). The gas blockage issues in centrifugal pumps have been overcome by (i) helico-axial pumps, where the pump geometry and impeller blades are designed to minimize the radial component of flow, so that liquid and gas are transported axially (ii) mutli-vane centrifugal pumps, where the vanes are split with large gaps such that the pressure distribution is altered and gas accumulation is avoided (iii) twin screw pumps, where meshing helical screws are used. As they rotate, the intermeshing screws form many chambers with the pump housing, and transport liquid and gas from the suction side to the discharge side. These pumps can handle large gas flow fractions (up to 75-98%). Positive displacement pumps are also used for gas-liquid flows. These include gear, peristaltic and piston pumps; the twin-screw pumps mentioned above also share some positive-displacement characteristics.

Many of these pumps used in the oil industry are quite large, but in principle can work for smaller applications. Since these pumps operate under a wide range of gas flow fractions in normal gravity, and consequently flow regimes, we do not expect any issues due to the reduction in the g-level (see, for example, [65] and [66].

7 Startup, transients and system instabilities

While the behavior of a two-phase flow system at steady state might be of ultimate interest to a designer, it is important to understand the characteristics of the system during startup or shutdown. When the system is started up from a quiescent state, the two phase flow will likely progress through flow regimes that are different from what prevails at steady state. For example, if an annular flow is desired at steady state and a transfer line is initially filled with liquid, the line would undergo bubbly flow and slug flow before an annular flow regime is achieved. The system or the component must be capable of withstanding any pressure oscillations or structural loads that might arise. Transients refer to time dependent behavior in general, which may ultimately die out and lead to steady behavior of the system, or to unexpected, unstable or catastrophic end state. Benign transients, especially near a steady state, can be fairly well understood by assuming the system behavior to be quasistatic, as is discussed later. Basically the system behavior is mapped assuming that it is at a steady state corresponding to the instantaneous flow condition.

Startup is particularly critical for heat pipes and capillary flow loops which work on the principle of meniscii being present in the wicked structures in the evaporator and condenser sections,

where phase change occurs. If the system is initially cold, the liquid may not be pumped adequately if the liquid viscosity changes appreciably with temperature, or the wick structures are flooded, or frozen as in the case of a high temperature liquid metal being the working fluid.

Transient system behavior can also lead to instabilities that are undesirable. Numerous components in fluid systems may be found to be associated with instabilities at the system level in the literature. For example, in a propulsion system "pogo" instability, space vehicle vibrations can produce oscillatory flow in the fuel feed line. This leads to thrust oscillations, which can feedback and couple with the fuel feed oscillations [67]. Pump cavitation and the resultant altered nature of the oscillation modes are compounding factors in pogo oscillations.

We discuss a few system instabilities in the rest of this section. While the nature of the instability can be clearly illustrated using simple physical arguments, the exact details of how it develops depends, necessarily, on the specifics of the system. For this reason we will not address here specific system configurations. Rather, we will focus on the physical nature of selected instabilities, and present simple 'toy model' calculations when feasible to understand basic dynamics and reveal general rules to avoid or get out of instabilities.

Instabilities are usually classified as static or dynamic, depending of whether the oscillation time scale is long (low frequency) or short (high frequency) compared with the characteristic time scale of the system. If the oscillation frequency is low, the system can track closely the system static operation –hence 'quasistatic instability'. If the oscillation frequency is high, the response cannot be examined using quasistatic approximations, and it usually becomes a complex function of frequency. Brennen [68] has a good summary of system instabilities in his book Fundamentals of Multiphase Flows. While some interesting instabilities are gravity-dependent (e.g., the 'geyser' instability), here we focus attention on those that are gravity-independent.

7.1 Ledinegg instability

7.1.1 Basic principles and simple model

This important instability occurs in a line (pipe)-pump system where the fluid changes phase due to heat input. Fig. 8 shows the pressure drop versus mass flow rate $\dot{m}$ for a pure vapor and a pure liquid flowing in a given piping line, together with a typical pump characteristic. The intersection of the pump and the line characteristics gives the operation point of the system. Assuming quasistatic conditions, it can easily be verified that if Δp_{line} increases with $\dot{m}$, then a small perturbation from the operating point will decay back to that point. Conversely, if the line Δp_{line} decreases with $\dot{m}$, the operation is unstable.

Since $\Delta p \sim \rho u^2 = \dot{m}^2/\rho$, the pressure drop for vapor is higher than for liquid for a given value of $\dot{m}$. If the heat input is independent of flow rate, the flow will be close to all-vapor at low $\dot{m}$ and close to all-liquid at high $\dot{m}$. At intermediate $\dot{m}$ the pipeline loss line must transition from vapor to liquid, and the shape of this transition determines whether an instability will occur. Specifically, if the transition exhibits the sigmoidal shape shown in fig. 8, the operation at point O is unstable.

In this section, we propose a simple model where $\Delta p_{\text{line}}(\dot{m})$ has a region of negative slope. The model assumes that liquid at temperature $T_i (\leq T_{\text{sat}})$ enters a pipe under constant heat flux q. We further assume no gradients in the radial direction, straight pipe line, and the following mixing rules for density and viscosity as a function of mass quality χ and the pure liquid and vapor properties

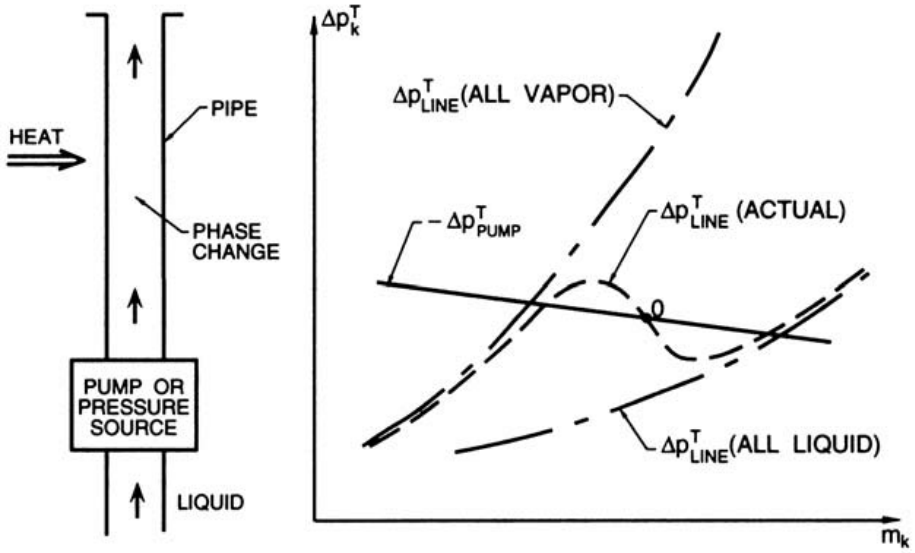

Figure 8: Schematic of Ledinegg instability. (From Brennen [68].)

(denoted by subscripts L and V) [7]:

$$\mu = (1-\chi)\mu_L + \chi\mu_V$$
$$\frac{1}{\rho} = \frac{1-\chi}{\rho_L} + \frac{\chi}{\rho_V}. \tag{68}$$

To calculate the pressure drop, we note that if liquid enters subcooled, there will be an initial pipe length

$$L_i \equiv \frac{\dot{m}\rho_L c_p(T_{\text{sat}} - T_i)}{\pi D q} \tag{69}$$

with all-liquid flow in $z < L_i$ and the liquid temperature being raised to T_{sat}. For pipes longer than

$$L_{\text{max}} \equiv L_i + \frac{\dot{m}\lambda}{\pi D q}, \tag{70}$$

where λ is latent heat, the flow in $z > L_{\text{max}}$ is all-vapor, with temperature rising above T_{sat}. Finally, for $L_i < z < L_{\text{max}}$ the flow is two-phase with $T = T_{\text{sat}}$.

There are friction and acceleration pressure drops. We model the friction pressure drop with a friction factor, f_ϕ, assumed constant,

$$\left.\frac{dp}{dz}\right|_f = -\frac{2}{D} f_\phi \frac{G^2}{\rho} = \frac{32 f_\phi}{\pi^2 D^5}\dot{m}^2 \left(\frac{1-\chi}{\rho_L} + \frac{\chi}{\rho_V}\right), \tag{71}$$

where $G \equiv \rho U = \frac{\dot{m}}{A} = \frac{4\dot{m}}{\pi D^2}$ is the mass velocity. This equation may be integrated by noting that, from a heat balance,

$$\begin{aligned} &\chi = 0, && z \le L_i \\ &\chi = \frac{\pi q D(z - L_i)}{\dot{m}\lambda}, && L_i \le z \le L_{\text{max}} \\ &\chi = 1, && z \ge L_{\text{max}} \end{aligned} \tag{72}$$

Property	Liquid	Vapor
μ (kg/m.s)	10^{-3}	2×10^{-5}
ρ (kg/m^3)	1000	0.58
c_p (J/kg.K)	4.2×10^3	—
λ (J/kg)	2.5×10^6	
q (W/m^2)	1.5×10^5	
T_{sat} (K)	100	
D (m)	10^{-2}	
f (fr. factor)	0.002	

Table 1: Fluid properties and pipe diameter assumed in our model.

The acceleration pressure drop accounts for the momentum change due to quality increase down the pipe; starting from $dp/dz = -\rho\, u\, du/dz$, it may be written as

$$\left.\frac{dp}{dz}\right|_a = G^2 \frac{d}{dz}\left(\frac{1}{\rho}\right) = G^2\left(\frac{1}{\rho_L} - \frac{1}{\rho_V}\right)\frac{d\chi}{dz}. \tag{73}$$

Since $d\chi/dz = \pi D q/\lambda\dot{m}$ by the heat balance in eq. 72, we get,

$$\left.\frac{dp}{dz}\right|_a = \frac{16\dot{m}^2}{\pi^2 D^4}\left(\frac{1}{\rho_L} - \frac{1}{\rho_V}\right)\frac{\pi q D}{\dot{m}\lambda} \qquad \text{for the 2-phase region, and} \tag{74}$$

$$\left.\frac{dp}{dz}\right|_a = 0 \qquad \text{for the single-phase regions.} \tag{75}$$

7.1.2 Model results

We have assumed the properties of liquid water and vapor and typical values for heat input q and pipe diameter D as shown in table 1.

Figs. 9-10 show that the pressure drop versus mass flow rate has a region of negative slope, therefore the Ledinegg instability can develop. The maximum pressure drop occurs at $\dot{m} = \dot{m}^*$. Fig. 9 shows the effect of inlet temperature. As T_i approaches T_{sat} the maximum location moves to larger $\dot{m}$. There is an inlet temperature T_i^* such that for $T_i > T_i^* \approx 98.8°$C there is no region of negative slope and therefore the Ledinegg instability cannot develop. At high $\dot{m}$ the plots merge with the all-liquid pressure drop —which is independent of temperature and only depends on L and $\dot{m}$.

Fig. 10 shows the effect of pipe length in a log-log plot. As $\dot{m} \to \infty$ the flow approaches the all-liquid pressure drop characteristic. The flow approaches the vapor theory at low $\dot{m}$, where the flow has a tiny liquid region, followed by an also small 2-phase region, and spending the time in most of the pipe as vapor. This implies that the slope cannot be that of the vapor-only pressure drop.

In conclusion, for typical liquid and water vapor properties, a simple model shows that conditions leading to Ledinegg instability are present for subcooled feeds, up to about 98.8°C; and that these conditions disappear for higher feed temperatures.

7.2 Concentration waves

This is not strictly an instability but it will give rise to a fluctuating unsteady operation. Assume that a closed flow loop with a pump develops a region of slightly different vapor quality. In fig. 11 (after

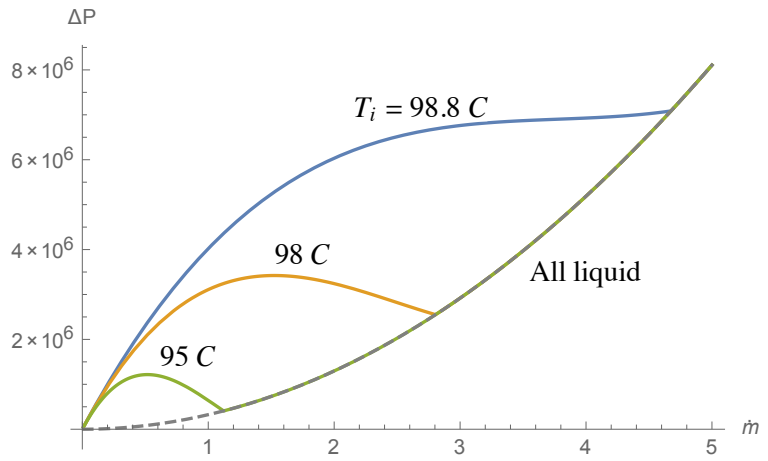

Figure 9: Effect of inlet temperature T_i on pressure drop versus mass flow rate $\dot{m}$. $L = 40$ m. The system would develop Ledinegg instability. The maximum pressure drop depends on T_i and it occurs at $\dot{m} = \dot{m}^*$. At high $\dot{m}$ the flow is all-liquid and the pressure drop follows the all-liquid line. Regions of $d\Delta p/d\dot{m} < 0$ cease to exist for $T_i \gtrsim 98.8°$C.

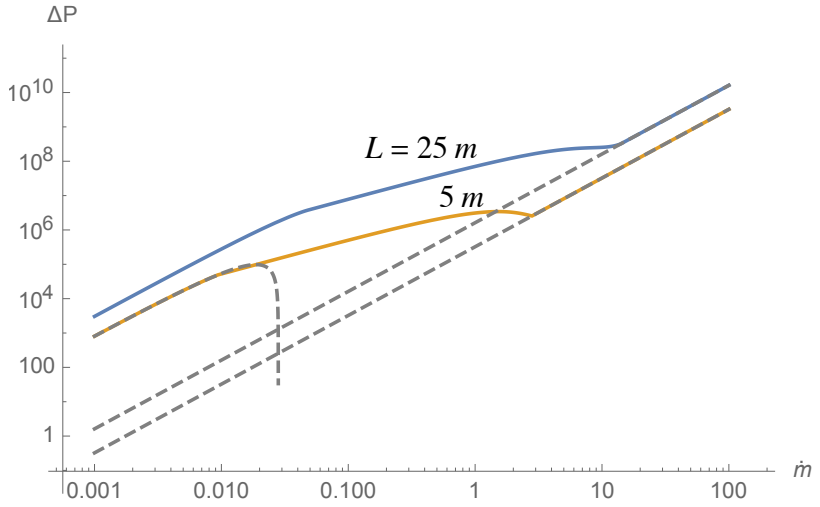

Figure 10: Effect of line length on pressure drop versus mass flow rate $\dot{m}$. $T_i = 98°$C. The pressure drop follows the all-liquid theory at high $\dot{m}$ and the all-vapor theory at low $\dot{m}$. The 5 m line has a region of negative slope, thus may develop Ledinegg instability. The 25 m line does not have a negative slope region. Negative slopes cease to exist for $L \gtrsim 13$ m.

Brennen [68]) we can see the line and the pump characteristics for each quality, χ and $\chi + \Delta\chi$. Assume that the concentration perturbation is slow to homogenize compared with the time of flow around the loop; and that the volume of the perturbation is such that it either resides in the line or in the pump. It is then obvious from fig. 11 that the operation will fluctuate between points A and B, with a frequency close to the time needed for the perturbation to go around the loop. This unstable operation may be avoided through the use of mixing devices or given sufficient time.

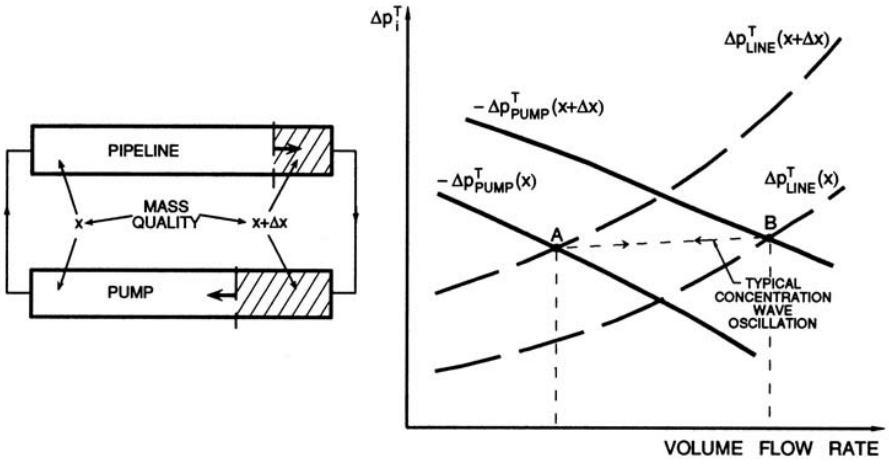

Figure 11: Schematic concentration wave. (From Brennen [68].)

7.3 Dynamic instabilities: cavitation

Following the discussion in Brennen, the cavitation instability is a true dynamic instability because it develops even though the slope of the pump Δp vs. flow rate characteristic is negative, which implies the system is quasistatically stable. The main points are:

-The phenomenon is observed more often in axial pumps, but has been observed in centrifugal pumps as well. The presence of dissolved gas can cause similar effects as gas comes out of solution.

-The phenomenon develops when the cavitation number

$$N_c \equiv \frac{2(p_i - p_v)}{\rho_L R_i^2 \Omega^2}, \tag{76}$$

(where p_i, p_v are the inlet and vapor pressures, and R_i, Ω the impeller radius and rotation rate) is smaller than a threshold that depends on the system.

-Dimensional analysis reveals that the cavitation surge frequency ω_i must have a dependence

$$\frac{\omega_i}{\Omega} = f(N_c, \phi, \text{type of pump}), \tag{77}$$

where $\phi \equiv (Q/A_d)/(\Omega R_i)$ is the flow coefficient for given volumetric flow Q and discharge area A_d. Empirical data suggests that the dominant variation is with cavitation number, and $\omega_i/\Omega \approx \sqrt{2\,N_c}$ is a crude approximation to the surge frequency.

8 Other topics

8.1 Flow metering and mass gauging

The measurement of two-phase flow flowing in a tube is a difficult issue both in normal and reduced gravity. Flow measurement is typically accomplished using spinning flow meters, Coriolis flow meters, differential pressure measurement, etc. Spinning flow meters, such as gear and turbine, work

on the principle of momentum exchange between the flow and the meter and thus depends on the flow velocity and density. In single phase flows, the fluid density is known, and the unknown quantity is the velocity, which is measured by the meter. In two-phase flows, the flow density depends on the amount of gas and liquid (or the void fraction) and a single measurement cannot determine both the density and velocity. The situation is similar for the differential pressure measurement.

A Coriolis flow meter measures the response in one or more oscillating curved tubes, due to a flow within it. The amount of mass in the tube (and thus the flow density) is determined by the natural frequency of the tube, and the phase shift in upstream and downstream sensors in the tube detects the mass flow rate. Thus, in principle, Coriolis flow meters can be used for two-phase flow. In practice, however, the flow regime (especially slug flow) alters the rate of damping of flow oscillations internal to the tube, and it is believed that measurement of two-phase flow is problematic for gas flow fractions in excess of 20-30%. Henry *et al.* [69] came up with an empirical methodology to correct the raw readings of a given Coriolis flow meter and a given flow mixture to come up with reliable measurements for gas void fractions up to 80%. The area of two-phase flow measurement using Coriolis meters is still one of active research. We note that there is at least one flow meter commercially available (OPTIMASS 6400, www.krohne.com) whose specification datasheet mentions "high performance with air entrainment, delivering continuous measurement even with 0-100% gas entrainment."

Assuming that a Coriolis flow meter has been thoroughly tested under normal gravity, no issues are anticipated in low gravity, as all the microgravity flow regimes would occur under normal gravity testing as well.

Void fraction is an important quantity in two-phase flows. It refers to the fraction of gas in the system, and can be defined globally in the entire two-phase system, or locally at locations of interest. It can be measured based on the fraction of gas along a line, in a cross-sectional area, or in a given volume of the two-phases. The void fraction can be measured using a variety of techniques – radiation attenuation, electrical contact probes, impedance measurements using capacitance or conductance sensors, or mechanically using quick-closing valves (Bertani *et al.* [70], Ahmed [71]). Quick-closing valves are not suitable in low gravity because the individual measurement of liquid and gas volumes relies on gravity for phase separation.

Electrical contact contact probes and other wet/dry sensors rely on the difference in physical properties of a gas and liquid to determine what fluid is in contact with the probe. Capacitance probes are quite attractive and have been used widely for void fraction measurements. The probes can be intrusive, for example installed as a wire mesh within the flow (Prasser *et al.* [72]) to detect the capacitance on a grid in one plane, or non-invasive by mounting the electrodes on the tube wall (Warsito and Fan [73], Ahmed [71]). Ahmed used both ring type and concave electrodes mounted on the outside of a tube to measure void fraction in air-oil flows. For properly designed electrodes, he found that the volume averaged void fraction in the measurement volume is independent of the flow regime in the tube (for annular, stratified, slug and elongated bubble flow); however, this is unlikely to be true in general. Furthermore, Ahmed found that the power spectrum density of the unsteady void fraction signals could be used to discern the flow regime. Wang *et al.* [74] have reviewed the design and applications of 2D and 3D electrical capacitance tomography for two-phase flows. Tomography refers to the reconstruction of phase distribution in a domain obtained from measurements taken from sensors placed outside the measurement volume. The sensor shape, electrode configuration and number of electrodes are key elements of capacitance sensors used for tomogra-

phy. Twelve electrodes are commonly used, giving sixty six independent capacitance measurements between each pair of electrodes. Image reconstruction is a major issue, and Wang discusses the current techniques used.

Mass gauging is important to determine the amount of fuel left in partially spent cryogenic fuel tanks in low gravity. This is a practically non-existent problem in normal gravity, as the liquid settles to the bottom of the tank. The height of the liquid in the tank, together with the tank geometry readily determines the amount of liquid. In low gravity, the ullage(s) could be present anywhere in the tank, and the tank walls could be wetted by the liquid. Thruster firings to temporarily settle the liquid together with wet/dry sensors within the tank were used early on in rocketry. Modern methods of mass gauging include (i) PVT techniques (Van Dresar, [75]) which uses the measured temperature and pressure of a pressurant gas (helium) in the fuel tank as well as the pressurant supply tank to determine the pressurant mass and density in the ullage, and ultimately the volume of the ullage in the fuel tank (ii) radio frequency mass gauging which uses the measured electromagnetic resonance frequencies of tank eigenmodes to gauge the amount of liquid in the tank [76].

8.2 Flow through porous media

Two-phase flow in porous media has been and still is very much a research topic, and has important economic impact for a number of industries –oil exploration and production, pharmaceutical, consumer products such as powdered detergents, and personal products such as diapers and feminine pads. While laminar, single-phase flow in porous media is properly described by Darcy's equation [77],[3] two-phase flow models lack theoretical backing and have to rely on semi-empirical concepts such as relative permeability.

In this section we discuss experimental results that show how gravity level affects the characteristics of gas-liquid flow in a packed column, a kind of a porous medium with a (rather large) millimetric pore size. The experiments have been performed over a period of about 15 years in parabolic flight campaigns aboard the various airplanes in service during that time. We address the effects of zero-gravity on pressure drops and on parametric boundaries between flow regimes.

8.2.1 Friction factors and pressure drop

Using the ideas of friction factor for straight tubes, the laminar velocity $\mathbf{u}$ of a fluid of viscosity μ flowing through a packing of effective size D_p is expressed by the Blake-Kozeny equation [79]:

$$\mathbf{u} = -\left[\frac{D_p^2 \epsilon^3}{150(1-\epsilon)^2}\right]\frac{\nabla p}{\mu}, \tag{78}$$

where the term in square brackets plays the role of Darcy's permeability, and ϵ is the porosity or gas-solid void fraction. In turbulent flow, the pressure drop is described with a constant friction factor, $f_t = 7(1-\epsilon)/8\epsilon^3$. In order to cover from laminar to turbulent flows, the laminar and turbulent pressure drops are added linearly, to yield the Ergun equation [79]:

$$\frac{-\Delta P}{L} = 150\left(\frac{\mu u}{D_p^2}\right)\frac{(1-\epsilon)^2}{\epsilon^3} + \frac{7}{4}\left(\frac{\rho u^2}{D_p}\right)\frac{1-\epsilon}{\epsilon^3}, \tag{79}$$

[3]Darcy's law gives the average point-wise velocity of the flow in terms of the permeability κ, viscosity μ and the average pressure gradient: $\mathbf{u} = -\frac{\kappa}{\mu}\nabla p$. The average is taken over a length scale much larger than the pore size but much smaller than the macroscopic size of the medium. While Darcy established this equation by careful experiments, Whitaker has developed a theoretical derivation based on volume-averaging [78]. For incompressible flow, $\nabla \cdot \mathbf{u} = 0$, which implies that the pressure satisfies the Laplace equation, $\nabla^2 p = 0$.

where $u \equiv |\mathbf{u}|$, ρ is density, and the pressure drop is understood as taking place in a straight duct over length L packed with particles of effective size D_p. In dimensionless form,

$$\frac{-\Delta P}{\rho u^2}\frac{D_p}{L}\frac{\epsilon^3}{1-\epsilon} = \frac{150}{Re}(1-\epsilon) + \frac{7}{4}, \tag{80}$$

where the left-hand side has the structure of a friction factor, and the Reynolds number is $Re \equiv u\rho D_p/\mu$.

When the flow is two-phase, these equations are no longer adequate. As gas and liquid are forced through the interstices of the packing, bubbles are deformed, squeezed, broken and reformed, all of which requires work —and therefore additional pressure drop. Motil [80] has developed a correlation valid for zero-gravity from data collected in parabolic flights which incorporates the flow of both phases and the phase interaction via surface tension into the single-phase Ergun equation (eqns. 79 or 80):

$$f_{TP} \equiv \frac{-\Delta P}{\rho_L U_{LS}^2}\frac{D_p}{L}\frac{\epsilon^3}{1-\epsilon} = \frac{1}{Re_{LS}}\left[150 + 0.8 Re_{GS}^{1/2}\left(\frac{Su_L}{Re_{LS}}\right)^{2/3}\right] + \frac{7}{4}, \tag{81}$$

where L, G, denote liquid or gas, and S denotes superficial velocity (or Reynolds number based on superficial velocity), and

$$Re_{LS} \equiv \frac{\rho_L U_{LS} D_p}{\mu_L(1-\epsilon)}, \quad Re_{GS} \equiv \frac{\rho_G U_{GS} D_p}{\mu_G(1-\epsilon)}, \quad Su_L \equiv \frac{\rho_L D_p \sigma}{\mu_L^2} \tag{82}$$

are the liquid and gas superficial Reynolds numbers, and the Suratman number, respectively. Figs. 12, 13 show the agreement of the model with data collected in low-gravity aircraft campaigns.

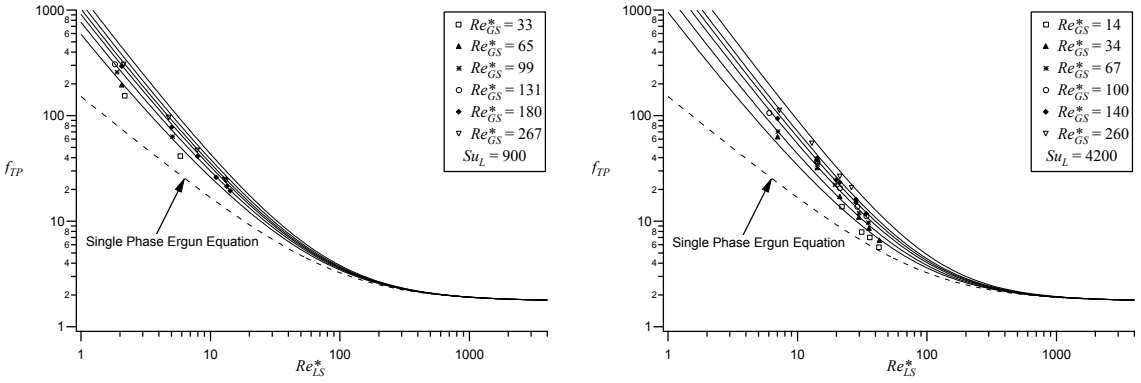

Figure 12: Low-gravity aircraft data and model from eq. 81 for $Su_L = 900$ and $Su_L = 4200$. (After Motil [80])

8.2.2 Flow regime maps

In two-phase contacting operations through packed columns, the flow regime greatly affects the efficiency of the transfer –e.g., heat, mass. Of the flow regimes that arise in normal gravity (trickle, bubbly, pulse and spray), only bubbly and pulse are relevant in zero-gravity. Trickle flow can only develop in a gravity environment as the liquid needs gravity to trickle down the column (while gas can either flow co- or counter-currently). And, while spray flow (where a mist of liquid droplets are

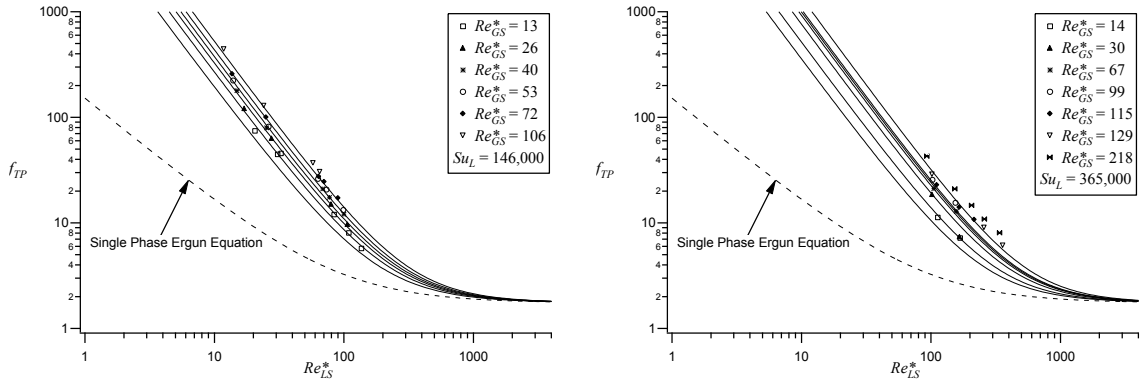

Figure 13: Low-gravity aircraft data and model from eq. 81 for $Su_L = 146000$ and $Su_L = 365000$. (After Motil [80])

entrained by the drag exerted by a fast-flowing continuous gas phase) can in principle develop in low gravity, it does only with extremely low liquid-to-gas flow rate ratios that make it impractical for normal operations. This leaves bubbly and pulse flows as the relevant types of flow in zero gravity.

Bubbly flow, a regime where gas bubbles are dragged by a continuous liquid phase, develops at relatively low gas flow rates for a given fixed liquid flow rate. As the gas flow rate increases, the flow transitions to pulse flow, which is quite similar to slug flow observed in smooth tubes. Pulse flow is characterized by an alternating sequence of packets or regions of gas-rich and liquid-rich flow. Pulse flow starts with 'weak' pulses that are not easily detectable by the naked eye through a transparent column. Well-developed pulses, on the other hand, are extremely clear and easy to spot by eye as a front between the gas- and liquid-rich regions, seen as a sharp change in brightness, moves downstream at a speed much higher than the fluid velocity.

Fig. 14 shows the bubbly-to-pulse transition plot extracted from Motil's low-gravity aircraft data [80]. The transition boundary is well approximated by the equation:

$$\frac{Re_{GS}}{Re_{LS}} = 700 \times Su_L^{-2/3}. \tag{83}$$

Comparing with eq. 13 for bubbly-slug transition in pipes, we note that eq. 83 exhibits the same power law of Su_L with a slightly larger coefficient. For details of flow regime transition maps in normal gravity, the reader is referred to the work of Güray Tosun [81].

8.2.3 Open aspects in zero-G

The following observations are offered after the recent operation in the ISS of the Packed Bed Reactor Experiment (PBRE), but are not intrinsic to zero-gravity necessarily.

1) When mixing gas and liquid to be injected into a packed column, formation of large gas bubbles in the liquid must be avoided by proper design of the mixing chamber. If large gas bubbles are allowed to form, the system pressure may develop oscillations with a period driven by the time between formation and dislodgement of the bubble. A properly designed mixing chamber should ensure that gas is always dispersed as bubbles of small enough size that pressure fluctuations are negligible –as determined by some science or technology requirement.

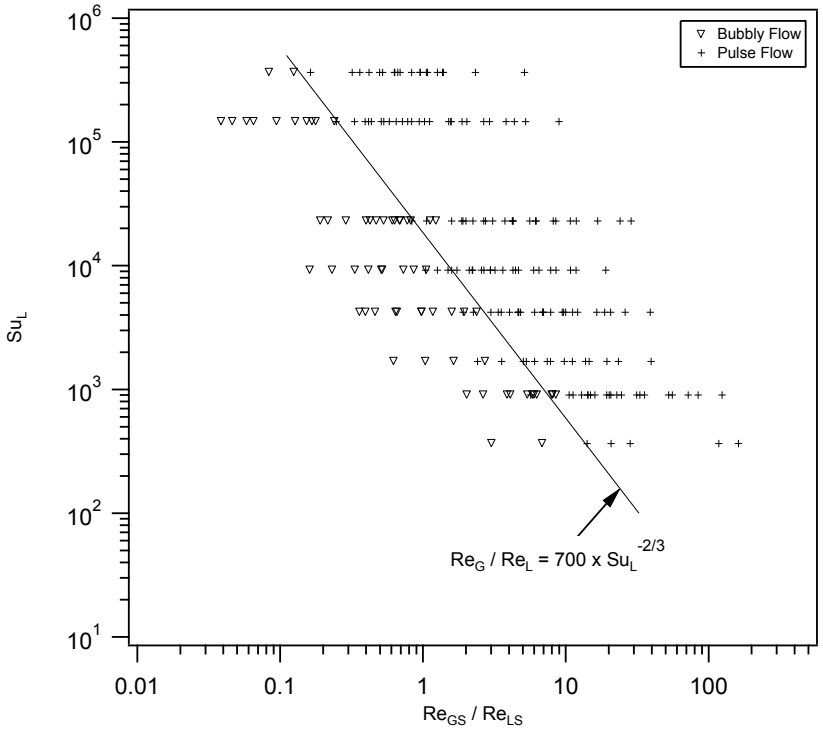

Figure 14: Low-gravity aircraft data showing the boundary between bubbly and pulse flow regimes. (After Motil [80])

2) In closed flow loops, oscillations downstream of the packed column may be fed back (or recycled) to the column inlet.

8.3 Heat pipes and capillary pumped loops

A heat pipe is a device used to transport heat from a heat source to a sink. The transfer of heat is efficient, and achieved with a high conductance (or low resistance), though the heat pipe and its components are themselves made of materials whose thermal conductivity is not very large. The latent heat of phase change of a pure working fluid during evaporation and condensation is used to achieve the efficient energy transfer. The heat pipe is a passive device; no external means are required for pumping the working fluid within it.

The principle of operation of a heat pipe is independent of gravity (refer to fig. 15). In its most common form, a heat pipe uses a porous wick to contain the working fluid in the liquid state. The pipe can be demarcated into three regions –the evaporation section where heat is added and vapor is generated, the adiabatic section in which the vapor transports the energy supplied, and the condenser section where heat is removed by external means causing the vapor to condense. The vapor temperature in these regions is nearly uniform, and the operating temperature depends on the heat load. The capillary pressure jump across the liquid/vapor interface in the pore of the wick in the evaporation section results in a higher pressure in the vapor than in the liquid. The vapor, with its increased enthalpy compared to the liquid, carries the energy supplied from the evaporator to the condenser section. There is a gentle pressure drop between these sections to drive the requisite

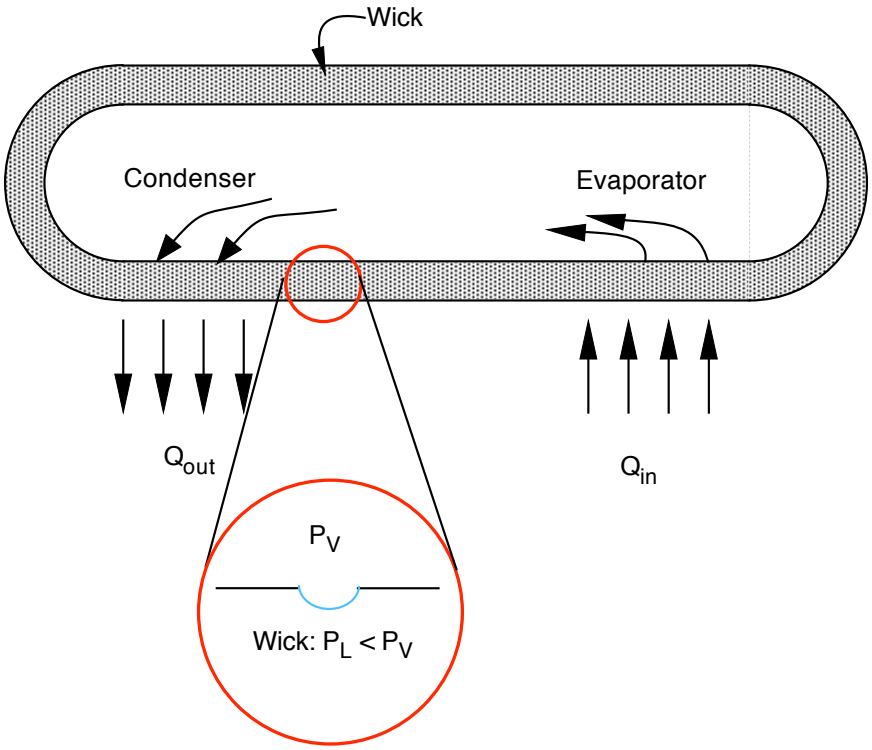

Figure 15: Schematic of a capillary heat pipe. Evaporation causes the meniscus to curve and create a pressure in the liquid that is below the pressure in the vapor. Vaporization sets a slight pressure gradient in the vapor phase that drives vapor to the condenser end. At the condenser, the meniscus curvature is smaller than in the evaporator; thus, the liquid pressure in the condenser is higher than in the evaporator.

vapor flow. A capillary pressure jump between vapor and liquid can also occur in the condenser section if the pores in the wick are not completely filled. The liquid returns to the evaporator from the condenser by a pressure gradient-induced return flow in the porous wick. For the heat pipe to work and the fluid to be pumped naturally, the capillary pressure jump in the evaporation section must be larger than that in the condenser section, so the condenser liquid pressure is greater than that at the evaporator. If the capillary pressure jump in the evaporator is unable to sustain the pressure differences necessary for the forward vapor flow and the liquid return flow, the heat load cannot be sustained. The evaporation section will become dry and the operation of the heat pipe will cease. This operation limit is termed the capillary limit of the heat pipe. Other operation limits also exist, viz., viscous limit, sonic limit, entrainment limit and boiling limit (see for example Reay *et al.*, [82]).

Looped heat pipes and capillary pumped loops also work on the same principle as described above. Fig. 16 shows a schematic of a capillary pumped loop. In a traditional heat pipe the vapor and liquid flow over each other in opposite directions. In looped devices, the vapor flow from the evaporator to the condenser, and the return flow of the liquid occur in separate paths in smooth pipes that form a closed circuit. A porous wick structure in the evaporator still provides the capillary pressure jump necessary to pump the fluid in the loop. The relatively high pressure drop of the liquid return flow in the wick in the traditional heat pipe is avoided in the looped devices. While the entrainment limit is absent as the vapor and liquid flow paths are distinct, other operation limits (capillary, sonic, etc) apply to looped heat pipes as well. The looped devices also contain a liquid reservoir or a compensation chamber.

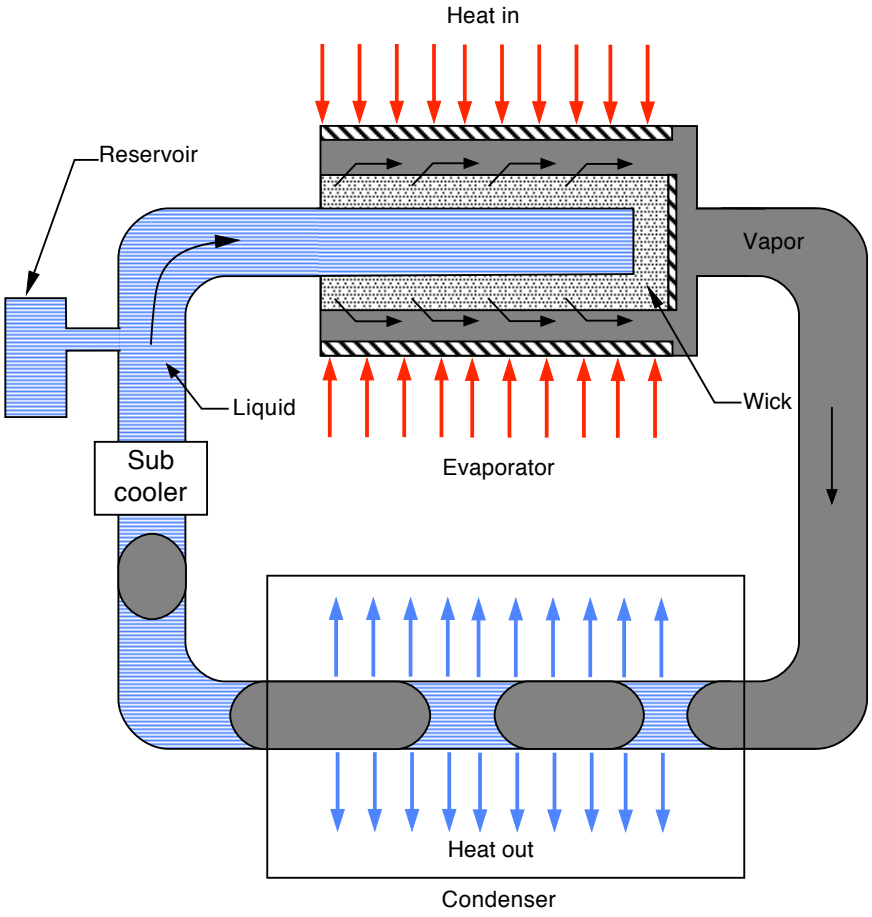

Figure 16: Schematic of a capillary pumped loop.

For traditional heat pipes the static Bond number (Eq 5), based on the wick pore size, is likely to be small in normal gravity. Hence the meniscus shape in the pores in normal and reduced gravity is unlikely to be significantly different. Gravity or a lack of it, however, can affect the pressure variation within the heat pipe, which must be considered in determining its operation. In the case of looped heat pipes, the two-phase flow regime in the condenser will be gravity dependent, and the pressure drop and heat transfer coefficients will likely be different for operation in normal and reduced gravity. The behavior of an idealized glass capillary pumped loop in low gravity was investigated by Hallinan and Allen [83] aboard the Space Shuttle Columbia in 1997. An unexpected failure mode was observed, wherein liquid collected and blocked the vapor return line, leading to dry-out of the evaporator. Analysis showed that liquid collection and blockage was due to instabilities of the liquid film that form due to condensation on the walls of the vapor return line. A wickless constrained vapor bubble heat pipe experiment using pentane was successfully performed by Plawsky and coworkers [84] on the International Space Station, showing significant differences in the heat pipe operation in microgravity compared to Earth's gravity. Specifically, the low gravity operation is affected favorably by increased liquid capillary flow, and the heat pipe operates at higher pressure and condenser temperature than on Earth, for the same heat load. The authors report that the interfacial heat transfer coefficient was an order of magnitude higher in low gravity due to the increased liquid flow rate.

Heat pipes have been designed and tested for a number of space applications. Shukla [85] and Swanson [86] provide a useful overview and historical perspective of many of the applications in space missions. Swanson mentions that the first operational capillary pumped loop was used aboard NASA's TERRA Spacecraft, launched in 1999. It has three scientific instruments that used capillary pumped loops, using ammonia, for tight temperature control with instrument heat loads in the range 25 to 264 W. Further details of the TERRA capillary pumped loops are available in Ku et al. [87].

References

[1] F.P. Chiaramonte and J.A. Joshi. Workshop on critical issues in microgravity fluids, transport, and reaction processes in advanced human support technology. TM 212940, NASA, 2004. AHST/UG Workshop, 2003.

[2] Committee for the Decadal Survey on Biological and Physical Sciences in Space, E. R. Cantwell and W. M. Kohrt, co-Chairs; National Research Council. *Recapturing a Future for Space Exploration: Life and Physical Sciences Research for a New Era*. National Academies Press, 2011.

[3] R.T. Lahey, Jr. and V. Dhir. Research in Support of the Use of Rankine Cycle Energy Conversion Systems for Space Power and Propulsion. Technical report, NASA/CR-2004-213142, 2004.

[4] G.F. Hewitt, G. Hetsroni, G. Yadigaroglu, S. Banerjee, and M. Ishii. Short course on modelling and computation of multiphase flows. Technical report, Swiss Federal Institute of Technology (ETH), Zurich, Switzerland, MAR 2005.

[5] R.T. Lahey. Short course: Transient multiphase flow and heat transfer at microgravity, Sept. 2002. NASA, Glenn Research Center, Cleveland, OH.

[6] C.J. Crowley and M.G. Izenson. Design Manual For Microgravity Two-Phase Flow and Heat Transfer. Technical report, Creare Inc. report prepared for Air Force Astronautics Laboratory, Air Force Space Technology Center, California, 1989.

[7] Issam Mudawar. Two-Phase Heat Transfer. Lecture Notes Prepared for NASA Glenn Research Center Short Course, December 2013.

[8] R. Balasubramaniam, E. Ramé, J. Kizito, and M. Kassemi. Two Phase Flow Modeling: Summary of Flow Regimes and Pressure Drop Correlations in Reduced and Partial Gravity. Technical report, NASA/CR-2006-214085, Cleveland, OH, 2006.

[9] Krotiuk, W.J., ed. Thermal-hydraulics for space power, propulsion and thermal management system design. In *Progress in Astronautics and Aeronautics*, volume 122. AIAA, 1990.

[10] International Space Station EVA Suit Water Intrusion: High Visibility Close Call. NASA, IRIS Case Number: S-2013-199-00005, Dec. 20, 2013.

[11] Spacewalk terminated due to spacesuit water leak. https://spaceflightnow.com/2016/01/15/spacewalk-terminated-due-to-spacesuit-water-leak/, 2016.

[12] Paul O. Wieland. Living together in space: the design and operation of life support systems on the International Space Station. Technical report, NASA Marshall Space Flight Center, 1998.

[13] G. Wölk, M. Dreyer, and H. J. Rath. Investigation on two-phase flow in small diameter non-circular channels in low and normal gravity. In *American Institute of Physics Conference Proceedings*, volume 458, pages 785–791, Space Technology and Applications International Forum, 1999.

[14] X. Fang, H. Zhang, Y. Xu, and X. Su. Evaluation of using two-phase frictional pressure drop correlations for normal gravity to microgravity to reduced gravity. *Advances in Space Research*, 49:352–364, 2012.

[15] J.F. Zhao, H. Lin, J.C. Xie, W.R. Wu, and Y. Zhang. Experimental study on pressure drop of two-phase gas/liquid flow at microgravity conditions. *J. Basic Sci. Eng.*, 9(4):373–380, 2001.

[16] E.K. Ungar, I.-Y. Chen, and S.H. Chan. Selection of a gravity insensitive ground test fluid and test configuration to allow simulation of two-phase flow in microgravity. In *Proceedings of the AIAA/ASME Joint Thermophysics and Heat Transfer Conference*, volume HTD-357-3, pages 71–78, Albuquerque, NM, June 14-18, 1998, 1998.

[17] H. Zhang, I. Mudawar, and M.M. Hasan. A method for assessing the importance of body force on flow boiling CHF. *Journal of Heat Transfer*, 126:161–168, 2004.

[18] S.S. Jayawardena, V. Balakotaiah, and L.C. Witte. Pattern transition maps for microgravity two-phase flows. *AIChE J.*, 43(6):1637–1640, Jun 1997.

[19] J. McQuillen. Microgravity Two-phase Flow. http://exploration.grc.nasa.gov/6712/2phase_flow/2phase.html.

[20] W. S. Bousman. *Studies of Two-phase Gas-Liquid Flow in Microgravity*. Ph.D. thesis, University of Houston, Feb 1995.

[21] C. Colin and J. Fabre. Gas-liquid pipe-flow under microgravity conditions - influence of tube diameter on flow patterns and pressure drops. *Adv. Space Res.*, 16(7):137–142, 1995.

[22] T. Takamasa, T. Hazuku, N. Fukamachi, Tamura N., Hibiki T., and Ishii M. Effect of gravity on axial development of bubbly flow at low liquid reynolds number. *Exp. Fluids*, 37(5):631–644, NOV 2004.

[23] T. Takamasa, T. Iguchi, T. Hazuku, T. Hibiki, and M. Ishii. Interfacial area transport of bubbly flow under microgravity environment. *Int. J. Multiphase Flow*, 29(2):291–304, FEB 2003.

[24] Airam Sausen, Paulo Sausen, and Mauricio de Campos. The slug flow problem in oil industry and pi level control. In Dr. Jorge Salgado Gomes, editor, *New Technologies in the Oil and Gas Industry*, chapter 5. InTech, DOI: 10.5772/50711, 2012.

[25] O. Kvernvold, V. Vindøy, T. Søntvedt, A. Saasen, and S. Selmer-Olsen. Velocity distribution in horizontal slug flow. *Int. J. Multiphase Flow*, 10(4):441–457, 1984.

[26] A. Kawahara, P.M.-Y. Chung, , and M. Kawaji. Investigation of two-phase flow pattern, void fraction and pressure drop in microchannels. *Int. J. Multiphase Flow*, 28:1411–1435, 2002.

[27] F. P. Incropera and D. P. De Witt. *Fundamentals of heat and mass transfer*. 'John Wiley & Sons, New York', 1985.

[28] M.M Awad and Y. S. Muzychka. A simple two-phase frictional multiplier calculation method. In *Proceedings of IPC 2004 International Pipeline Conference*, pages 1–9, October 4-8, 2004, Calgary, Alberta, Canada, Oct 2004.

[29] C. Colin, J. Fabre, and J. McQuillen. Bubble and slug flow at microgravity conditions: state of knowledge and open questions. *Chem. Eng. Commun.*, 141:155–173, 1996.

[30] S-Y. Son and J.S. Allen. Visualization of wettability effects on microchannel two-phase flow resistance. *Transactions of the ASME*, 126:498, Aug 2004.

[31] H. Wong, S. Morris, and C.J. Radke. Three-dimensional menisci in polygonal capillaries. *J. Colloid Interface Sci.*, 148(2):317–336, 1992.

[32] H. Wong and C.J. Radke. The motion of long bubbles in polygonal capillaries. part 1. thin films. *J. Fluid Mech.*, 292:71–94, 1995.

[33] H. Wong and C.J. Radke. The motion of long bubbles in polygonal capillaries. part 2. drag, fluid pressure and fluid flow. *J. Fluid Mech.*, 292:95–110, 1995.

[34] K.A. Triplett, S.M. Ghiaasiaan, S.I. Abdel-Khalik, and D.L. Sadowski. Gas-liquid two-phase flow in microchannels. Part I: two-phase flow patterns. *Int. J. Multiphase Flow*, 25:377–394, 1999.

[35] I. Chen, R. Downing, E.G. Keshock, and M. Al-Shariff. Measurements and correlation of two-phase pressure drop under microgravity conditions. *Journal of Thermophysics and Heat Transfer*, 5(4):514–523, 1991.

[36] J. F. Zhao, H. Lin, J. C. Xie, and W. R. Hu. Pressure drop of bubbly two-phase flow in a square channel at reduced gravity. *Advances in Space Research*, 29(4):681–686, 2002.

[37] K. Gabriel. *Microgravity Two-phase Flow and Heat Transfer*. Microcosm Press/ Springer, 2007.

[38] M. Narcy and C. Colin. Two-phase pipe flow in microgravity with and without phase change: Recent progress and future prospects. *Interfacial Phenomena and Heat Transfer*, 3(1):1–17, 2015.

[39] L. Preziosi, K. Chen, and D.D. Joseph. Lubricted pipelining: stability of core-annular flow. *J. Fluid Mech.*, 201:323–356, 1989.

[40] J.P. Holman. *Heat transfer*. 'McGraw Hill, New York', 1976.

[41] J.G. Knudsen and D.L.V. Katz. *Fluid dynamics and heat transfer*. McGraw-Hill series in chemical engineering. McGraw-Hill, 1958.

[42] D. Chisholm. A Theoretical Basis for the Lockhart-Martinelli Correlation for Two-Phase Flow. *Int. J. Heat and Mass Transfer*, 10:1767– 1778, 1967.

[43] D.D. Hall and Issam Mudawar. Critical heat flux (CHF) for water flow in tubes-II. Subcooled CHF correlations. *Int. J. Heat Mass Transfer*, 43:2605–2640, 2000.

[44] J. C. Chen. A Correlation for Boiling Heat Transfer to Saturated Fluids in Convective Flow. *Ind. Eng. Chem. Process Des. Dev.*, 5(3):322–329, 1966.

[45] Sung-Min Kim and Issam Mudawar. Universal approach to predicting saturated flow boiling heat transfer in mini/micro-channels - Part II. Two-phase heat transfer coefficient. *Int. J. Heat Mass Transfer*, 64:1239–1256, 2013.

[46] J. Hart, J. Ellenberger, and P. J. Hamersma. Single- and two-phase flow through helically coiled tubes. *Chem. Eng. Sci.*, 43(4):775–783, 1988.

[47] A.S. Sangani, V.I. Kushch, M. Hoffmann, H. Nahra, D.L. Koch, and Y. Tsang. Behavior of rapidly sheared bubble suspensions. Technical Report NASA/TM-2002-211203, NASA, 2002.

[48] John B. McQuillen and Brian Motil. Reduced Gravity Gas and Liquid Glows: Simple Data for Complex Problems. Technical Report NASA/TM-2001-210681, NASA, 2001.

[49] Subash S. Jayawardena and John B. McQuillen. *Microgravity two-phase flow at a pipe junction*. AIAA Paper 96-2070. AIAA, Fluid Dynamics Conference, New Orleans, LA, June 17-20, 1996.

[50] Limin Yang, Zhenying Zhao, Pengcheng Qi, Lili Zhao, and Barry J. Azzopardi. Phase Separation of Gas-Liquid Two-Phase Flows in Multi-tube T-Junction Separators. pages 241–244. 2010 The Second China Energy Scientist Forum, 2010.

[51] D. Schrage, J. Shoemaker, and J. McQuillen. Passive two-phase fluid separation. In *Proceedings of the 36th Aerospace Sciences Meeting and Exhibition*, Reno, NV, 1998.

[52] M. Ellis, R. C. Kurwitz, and F. R. Best. Development of a Unique, Passive, Microgravity Vortex Separator. In *Proceedings of International Mechanical Engineering Congress and Exposition*, number IMECE2005-81616, pages 763–770, Orlando, Florida, USA, November 5-11, 2005, 2005. ASME.

[53] Nathaniel C. Hoyt, Ming-Fang Kang, Kuan-Lin Lee, Adel Kharraz, Jaikrishnan Kadambi, and Yasuhiro Kamotani. Study of steady and dynamic behavior of gas core of passive cyclonic separator for space applications. *Microgravity Sci. Technol*, 25:187–200, 2013.

[54] Xiongjun Wu, Greg Loraine, Chao-Tsung Hsiao, and Georges L. Chahine. Development of a passive phase separator for space and earth applications. *Separation and Purification Technology*, 189:229 – 237, 2017.

[55] M.M. Weislogel, E.A. Thomas, and J.C. Graf. A Novel Device Addressing Design Challenges for Passive Fluid Phase Separations Aboard Spacecraft. *Microgravity Sci. Technol.*, 21:257–268, 2009.

[56] Ryan M. Jenson, Andrew P. Wollman, Mark M. Weislogel, Lauren Sharp, Robert Green, Peter J. Canfield, Jörg Klatte, and Michael E. Dreyer. Passive phase separation of microgravity bubbly flows using conduit geometry. *Int. J. Multiphase Flow*, 65:68–81, 2014.

[57] Jie Xu, Regis Vaillant, and Daniel Attinger. Use of a porous membrane for gas bubble removal in microfluidic channels: physical mechanisms and design criteria. *Microfluid. Nanofluidics*, 9(4):765–772, 2010.

[58] John B. McQuillen, Terri L. McKay, DeVon W. Griffin, Dan F. Brown, and John T. Zoldak. Final Report for Intravenous Fluid Generation (IVGEN) Spaceflight Experiment. Technical Report NASA/TM—2011-217033, NASA, 2011.

[59] Neil C. Dias, Marc D. Porter, and James S. Fritz. Principles and applications of colorimetric solid-phase extraction with negligible depletion. *Anal. Chim. Acta*, 558(1-2):230–236, 2006.

[60] R. Shankar Subramanian and R. Balasubramaniam. *The Motion of Bubbles and Drops in Reduced Gravity*. Cambridge University Press, 2001.

[61] D. El Sherif and J. Knox. International Space Station Carbon Dioxide Removal Assembly (ISS CDRA) Concepts and Advancements. SAE Technical Paper 2005-01-2892, 2005.

[62] Gong Hua, Gioia Falcone, Catalin Teodoriu, and Gerald L. Morrison. Comparison of Multiphase Pumping Technologies for Subsea and Downhole Applications. *Oil and Gas Fac.*, 1(5):36–46, 2012.

[63] Maryam Khalili, Akbar Alidadi Shamsabadi, Mahdi Mohammadi Janaki, and Daryosh Mohammadi Janaki. Examination of Application and Function of Two-phase Pumps. *Indian J. Sci. Technol.*, 7(5):1153–1163, 2014.

[64] Paul Cooper, Bruno Schiavello, Jacques de Salis, Charles D. Marolles, Allan J. Prang, and Dan Broussard. Multiphase gas-liquid pumping. In *13th International Pump User Symposium (1996)*, pages 159–174. Texas A&M University, 1996.

[65] Vance Havens and Dana Ragaller. Study of toluene rotary fluid management device and shear flow condenser performance for a space-based organic rankine power system. Technical report, National Aeronautics and Space Administration, CR-180885, 1988.

[66] Wayne S. Hill and Frederick R. Best. Microgravity two-phase flow experiment and test results. In *SAE Technical Paper*. SAE International, 1991.

[67] Several authors. Prevention of coupled structure-propulsion instability (pogo). Technical Report NASA/SP-8055, NASA, 1970.

[68] Christopher Brennen. *Fundamentals of Multiphase Flows*. Cambridge University Press, 2005.

[69] Manus Henry, Michael Tombs, Mihaela Duta, Feibiao Zhou, Ronaldo Mercado, Frank Kenyery, Joseph Shen, Martin Morles, Carlos Garcia, and Robbie Langansan. Two-phase flow metering of heavy oil using a Coriolis mass flow meter: A case study. *Flow Meas. Instrum.*, 17(6):399–413, 2006.

[70] C. Bertani, M. De Salve, M. Malandrone, G. Monni, and B. Panella. State-of-art and selection of techniques in multiphase flow measurement. Technical Report RdS/2010/67, Agenzia Nazionale per le Nuove Tecnologie, l'Energia e lo Sviluppo Economico Sostenibile, Ministero dello Sviluppo Economico, Italy, 2010.

[71] H. Ahmed. Capacitance Sensors for Void-Fraction Measurements and Flow-Pattern Identification in Air-Oil Two-Phase Flow. *IEEE Sensors J.*, 6(5):1153–1163, 2006.

[72] H.-M. Prasser, M. Misawa, and I. Tiseanu. Comparison between wire-mesh sensor and ultrafast x-ray tomograph for an air–water flow in a vertical pipe. *Flow Measurement and Instrumentation*, 16(2-3):73–83, 2005.

[73] W. Warsito and L.-S. Fan. Measurement of real-time flow structures in gas-liquid and gas-liquid-solid flow systems using electrical capacitance tomography (ect). *Chem. Eng. Sci.*, 56:6455–6462, 2001.

[74] Fei Wang, Qussai Marashdeh, Liang-Shih Fan, and Warsito Warsito. Electrical capacitance volume tomography: Design and applications. *Sensors*, 10(3):1890, 2010.

[75] Neil T. Van Dresar. PVT gauging with liquid nitrogen. *Cryogenics*, 46(2-3):118–125, 2006.

[76] Gregory A. Zimmerli, Karl R. Vaden, Michael D. Herlacher, David A. Buchanan, and Neil T. VanDresar. Radio frequency mass gauging of propellants. Technical Report NASA/TM—2007-214907, NASA, 2007.

[77] Henry Darcy. *Les fontaines publiques de la ville de Dijon*. Victor Dalmont, Paris, 1856.

[78] Stephen Whitaker. Flow in porous media I: A theoretical derivation of Darcy's law. *Transport in Porous Media*, 1(1):3–25, 1986.

[79] R. Byron Bird, Warren E. Stewart, and Edwin N. Lightfoot. *Transport Phenomena*. John Wiley & Sons, Inc., 2nd edition, 2002.

[80] Brian J. Motil, Vemuri Balakotaiah, and Yasuhiro Kamotani. Gas-liquid two-phase flow through packed beds in microgravity. *AIChE J.*, 49(3):557–565, 2003.

[81] Güray Tosun. A study of cocurrent downflow of nonfoaming gas-liquid systems in a packed bed. 1. flow regimes: Search for a generalized flow map. *Ind. Eng. Chem. Process Des. Dev.*, 23:29–35, 1984.

[82] David Reay, Ryan McGlen, and Peter Kew. *Heat Pipes-Theory, Design and Applications, Sixth Edition*. Elsevier, 2014.

[83] K.P. Hallinan and J.S. Allen. Comments on the operation of capillary pumped looped devices in low gravity. In *4th Microgravity Fluid Physics and Transport Phenomena Conference*, Cleveland, Ohio, USA, August 11-14, 1998.

[84] A. Chatterjee, J.L. Plawsky, P.C. Wayner, D.F. Chao, R.J. Sicker, T. Lorik, L. Chestney, R. Margie andJ. Eustace, and J. Zoldak. Constrained vapor bubble heat pipe experiment aboard the international space station. *J. Thermophysics and Heat Transfer*, 27(2):309–319, 2013.

[85] K.N. Shukla. Heat pipe for aerospace applications-an overview. *Journal of Electronics Cooling and Thermal Control*, 5:1–14, 2015.

[86] T.D. Swanson. Thermal control technologies for complex spacecraft. In *Proceedings of the 13th IHPC*, pages 1–11, Shanghai, China, 2004.

[87] J. Ku, L. Ottenstein, D. Butler, T. Swanson, and D. Thies. Thermal Performance of Capillary Pumped Loops Onboard Terra Spacecraft. In *Proceedings of the 2004 ICES Conference*, Vigo, Spain, 2004.